

We thank the referee for taking the time to read our manuscript and for their helpful comments!

### General changes

- We have considerably changed the text throughout the manuscript to improve the logical order of the text and to improve the explanations and comprehensibility. We added new subsections and improved the use of the English language.

### Major comments

- A) **The novelty of this study is not apparent to me.**

The novelty is the explicit simulation of the upward transport of air parcels inside convective updrafts and of the variable residence time of air parcels in convection, in contrast to schemes which only redistribute air parcels from the entrainment to the detrainment locations in a fixed time step.

#### **Which elements of this convective transport scheme are standard, and which elements are new?**

The explicit simulation of the upward transport of air parcels inside convective updrafts is new, and the algorithm for detrainment has to be changed accordingly. The redistribution according to entrainment and detrainment probabilities, respectively, is standard. We have more clearly stated this in the description of the algorithm. See also the reply to two comments in major comment C below: comment to page 4, section 2.2 (entrainment) and comment to page 6, section 2.4 (detrainment).

#### **First, my impression was that the use of so-called random convective area fraction profiles is novel, but then this goes back to Gottwald et al. (2016)**

The stochastic parameterisation described in Gottwald et al. had so far not been implemented to estimate convective mass fluxes in convective transport models. The implementation of their method in a transport model is novel.

#### **The authors should discuss in greater detail how their scheme differs from existing schemes, e.g., the ones mentioned on p. 2 line 5.**

The scheme extends the approach in existing schemes by modelling vertical updraft velocities and the time that an air parcel spends inside the convective event. Apart from that, the convective transport part of all schemes (including our scheme), is similar (that is the redistribution of the air parcels given the entrainment rates, detrainment rates and mass fluxes). We hope that we have now more clearly stated the novelty and differences in the introduction and the description of the method.

- B) **There must be many studies about convective tracer transport, but very few of them are referenced and discussed.**

**The simulations of Radon-222 and SO<sub>2</sub> are not discussed in the framework of the existing literature.**

We have added discussion to section 4.4 (section 4.2 in the original manuscript) on how well the results of other studies compare to radon measurements to put the comparison of our model to radon measurements into perspective. Other studies show differences between their models and the radon measurements of a similar order of magnitude (Jacob et al., 1997, Collins et al., 2002, Forster et al., 2007, Feng et al., 2011). More discussion of the validation of convective transport models was added in the introduction and in the conclusions. The large uncertainties in emissions, measurements, chemistry and microphysics of short-lived species generally pose a challenge for the validation of the simulation of these species, which we think is an important issue. We have added Feichter and Crutzen (1990) as an additional study to the references.

We added a discussion of the implications of the differences in the simulation of SO<sub>2</sub> in the different sensitivity runs to section 5. In addition, we added a paragraph discussing very-short lived bromine species to show that the algorithm is also relevant for species other than SO<sub>2</sub>.

This is a technical paper presenting a new algorithm, which is intended as a technical reference to cite when this algorithm is used in an application. It is outside the scope of this paper to give a more detailed discussion of studies of convective tracer transport. Several review papers are cited in the manuscript for reference (e.g. Mahowald et al., 1995, Jacob et al., 1997, Hoyle et al., 2011).

*Changes to the manuscript:* Added discussion in the introduction and conclusions of the validation by radon and the issue that the uncertainties in measurements, chemistry, microphysics and emissions pose a challenge for the validation of the simulation of short-lived species. Added discussion to section 4.4 (section 4.2 in the original manuscript) on how well other models compare to the radon measurements. Added an additional reference (Feichter and Crutzen, 1990). Added discussion of the implications of the differences in the simulation of SO<sub>2</sub> to section 5 and added three new references (Feichter et al., 1996, Kremser et al., 2016, Rollins et al., 2017). Added discussion of very short-lived bromine species to section 5 and added three references (Hossaini et al., 2012, Schofield et al., 2011, Wales et al., 2018).

- C) **Page 1 line 1 and page 2, line 3: What is meant by ensemble trajectory simulations?**

We agree that it was not obvious what was meant.

*Changes to the manuscript:* We added the following explanation to the introduction: "In addition, the scheme can be used for applications such as

backward trajectories starting along flight paths or sonde ascents, where it allows for simulating the effect of convection when using a statistical ensemble of trajectories starting at every measurement location.”

**Page 2, line 16: Explain better what is meant by instantaneous redistribution**

The Lagrangian convective transport schemes cited here use a short fixed time step to redistribute air parcels, which is not necessarily the same as the advection time step. Collins et al. use a fixed time step of 15 minutes for convection and of 3 hours for large-scale advection. That is, the time period between entrainment and detrainment is fixed to 15 minutes. Forster et al. also use a 15 minute time step. Rossi et al. use a time step of 30 minutes.

*Changes to the manuscript:* We rephrased several parts of the abstract and the introduction to make that more clear. We replaced all occurrences of ”instantaneous redistribution” by ”redistribution in a fixed time step” to avoid misunderstandings.

**Page 3, lines 23 and 27: Unclear to me what exactly is meant by ”meteorological data”**

*Changes to the manuscript:* We changed ”meteorological data” or ”meteorological analysis” to ”meteorological analysis data” to make that more consistent throughout the paper and to make clear that we are referring to the same data.

**Page 4, section 2.2: Is this treatment of entrainment [...] standard, i.e., as in other schemes, or is there some novelty here?**

Yes, this part of the algorithm is standard, see e.g. Collins et al., 2002 and Forster et al., 2007.

*Changes to the manuscript:* We have added these references to the text.

**Page 6, section 2.4: Is this treatment of [...] detrainment standard, i.e., as in other schemes, or is there some novelty here?**

This part of the algorithm is not standard, since it explicitly simulates the upward transport of the air parcel inside the cloud. In other models, only the probability that an entrained air parcel detrains at a given altitude is calculated. The final probability that an air parcel detrains at a certain altitude is the same in our approach and the approach of Collins, Forster and Rossi.

*Changes to the manuscript:* Added to section 2.5 (section 2.4 in the original manuscript): ”The approach for detrainment described above differs from the approach employed in previous Lagrangian convective transport schemes, since it takes into account the explicit simulation of the time that air parcels spend in convective updrafts, whereas schemes such as those employed in Collins et al. or Forster et al. assume a constant time that parcels spend in convection. The probability that an entrained air parcel detrains at a given altitude, however, is the same in both approaches.”

**Page 7, line 26: This important statement (?) requires much better explanation; it appears rather problematic that  $f_u$  is not in agreement with the actual number of trajectories in updrafts.**

This was not discussed properly and would leave the reader with the impression that there is a significant problem, which actually is not the case.  $f_{up}$  is very small, and the results of the validation runs show that the mass conservation is not noticeably affected by the uncertainty in the number of trajectories in convection.

As an alternative to  $f_{up}$ , the fraction of trajectory air parcels that are currently in convection in the model run could be used. This is however only possible for global runs. The mass flux of trajectories through a given surface is not necessarily balanced for non-global ensembles of trajectories. The approach would require to average the results over a volume that is small enough to allow for variations in the fraction, but large enough to contain a sufficient number of air parcels.

Another alternative would be to subsidize all air parcels and not only the air parcels, which are currently not in convection (see Collins et al., 2002). Subsiding air parcels which are currently in convection is however not only unphysical, but also can result in air parcels that descend while they are in convection and that possibly detrain at a lower altitude than they were entrained.

*Changes to the manuscript:* Extended discussion in section 2.6 (section 2.5 in the original manuscript) along the lines outlined above.

**Page 8, line 18: What type of radar measurements? Since this profile (Fig. 3) is important for this study, it would be important to understand better what it is based on.**

*Changes to the manuscript:* We added that the radar is a "precipitation radar" and that the profile is based on the data of two wet seasons (2005/2006 and 2006/2007). We added that the method to obtain the area fractions is "estimating the fraction of convection by comparing the area of convective precipitation to the total measured area".

**Page 10, line 3: I don't think that the character of the method is "random", most likely you mean "probabilistic" or "stochastic"**

*Changes to the manuscript:* Changed.

- D) My most important concern [...] How many air parcels / trajectories are required per reanalysis or GCM grid box in order to care about updrafts? [...]

There is a misunderstanding here, namely that the convective updraft area is needed to calculate the number of trajectories affected by convection in a given time period or the probability for a trajectory going into convection, which is not the case! Possibly, this misunderstanding was caused by the formulation "since a grid box contains several convective systems that only

cover a small fraction of the grid box, a statistical approach is necessary” (page 3, lines 1–2). This was misleading and has been rephrased.

The convective area fraction is not needed for calculating entrainment and detrainment probabilities and the probability is independent of the area covered by convection. It is *only* needed for the calculation of the vertical updraft velocities. Hence, it is not used in the descriptions of the other Lagrangian convective transport schemes (Collins, Forster, Rossi).

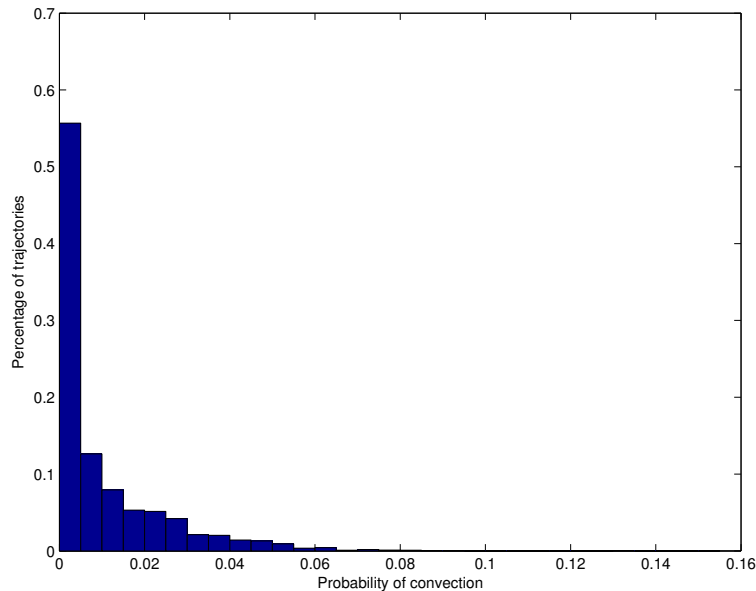
The quantity which is relevant for the entrainment probability is the entrainment rate integrated over altitude (with most entrainment typically at cloud base) and not the convective area fraction (see also discussion in section 2.2 of the original manuscript and Equation 3). It is only relevant how much air can be processed by entrainment in a given time period compared to the mass of the grid box. The probability of convection is therefore also dependent on the considered time period.

While the mass flux of the entrained air is proportional to the product of convective area fraction and vertical updraft velocity (see Equation 4 and discussion), these quantities are not needed for the calculation of the probabilities, which only depend explicitly on the entrainment rate. A small updraft velocity and a large convective area and a large updraft velocity and a small convective area lead to the same result for the entrainment rate.

The only place where convective area fractions are needed in the model are the vertical updraft velocities, which cannot be deduced from the mass fluxes alone. The only reason for this is that the mass fluxes in ERA Interim are given as grid-box means, while the mass flux inside the cloud is needed.

To show that the number of trajectories is sufficient to capture the updrafts, we calculated a frequency distribution of the probability that a trajectory is entrained into a convective cloud for all trajectories below 2 km from the first time step of the run in the tropical Pacific described in section 4.1. 77 % of the trajectories have a probability greater than zero to entrain into a convective cloud in a time period of 10 minutes. The mean probability for entrainment for an individual trajectory (including zero values) is 1 % and the maximum value is 13 %. The figure on the next page shows the frequency distribution.

The trajectories which have a probability greater than zero to entrain are distributed over about 1000 grid boxes. About 20 trajectories per grid box have an average chance of more than 1% (each) of entraining into a convective cloud within 10 minutes. It is clear from these numbers that not only at any given point in time, there is large number of trajectories capturing an updraft, but also that all individual grid boxes are covered well.



*Changes to the manuscript:* Changed formulation at page 3, lines 1–2 to: “Typical resolutions of meteorological analysis data are of the order of  $1^\circ \times 1^\circ$ . A grid box of the analysis typically contains several convective systems which only affect a small fraction of the mass contained in the grid box, which necessitates a statistical approach.”

**Maybe this issue is addressed on p. 4 line 4 (“The mass of a trajectory [...]”)**

Part of the issue is addressed here. The equations of the model are independent of the mass of the trajectory air parcel (for example, Equation 3). Thus, in a global model where the trajectories fill the model domain, a larger mass associated with a trajectory parcel (i.e. a lower density of trajectories per volume) leads to a lower number of trajectories in convection at a given point in time, which balances the higher mass moved per convective event.

Also, in response to a comment of the other reviewer, we considerably rephrased and extended the paragraph.

*Changes to the manuscript:* We considerably extended the discussion at the end of section 2.1 and moved the discussion to a new section 2.2 (in response to the other reviewer).

- **E) In the examples shown, timesteps of 10 or 30 min (why this difference?) have been chosen. I regard these timesteps as way too large to apply the approach outlined in sections 2.2–2.4: since updraft velocities can be up to  $20 \text{ m s}^{-1}$ , a timestep of 30 min injects a near-surface air parcel deep into the stratosphere. How can this work?**

The simulation time step inside the convective event is 10 seconds and not 10 minutes (e.g. original manuscript page 3, lines 12–15 and page 5, lines 9–14). The choice of the timestep is discussed under consideration of the updraft velocities on page 5, lines 13–14.

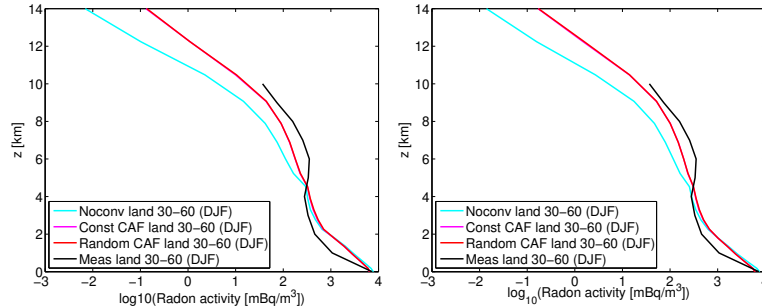
We are aware that the two time steps for the large scale advection outside convection ( $\Delta t$ ) and for the updraft inside convection ( $\Delta t_{\text{conv}}$ ) can easily be confused. We have now clarified some of the notation.

*Changes to the manuscript:* Clarified the notation. In particular, we have changed "trajectory time step" consistently to "advection time step of the trajectory model" and changed "intermediate time step" consistently to "convective intermediate time step".

**... timesteps of 10 or 30 min (why this difference?)...**

The difference is due to computational constraints. The long-time run comprises more than 15 years. Simulation time is considerably reduced by changing the time step from 10 min to 30 min without changing the results significantly (the time step is still much shorter than the lifetime of radon).

1-year runs with a time step of 10 minutes,  $0.75^\circ \times 0.75^\circ$  resolution of the analysis and a mean distance of the trajectories of 75 km have been performed to demonstrate that the results do not change significantly. They show that the runs with a time resolution of 30 min, a horizontal resolution of  $2^\circ \times 2^\circ$  and a mean distance of 150 km give nearly identical results (see figure, left:  $2^\circ \times 2^\circ$ , 30 min from Fig. 10 manuscript, right:  $0.75^\circ \times 0.75^\circ$ , 10 min).



In response to a comment of the other reviewer, we increased the resolution of the ERA Interim reanalysis to  $0.75^\circ \times 0.75^\circ$  for the high resolution run. In addition, the runs from section 4.1 and the  $\text{SO}_2$  run are based on ERA Interim  $0.75^\circ \times 0.75^\circ$  analysis data now.

*Changes to the manuscript:* Added to section 4.4 (section 4.2 in the original manuscript): "The change from 10 minutes to 30 minutes and from  $0.75^\circ \times 0.75^\circ$  to  $2^\circ \times 2^\circ$  is due to computational constraints. We performed 1-year test runs with  $0.75^\circ \times 0.75^\circ$  resolution, a 10 minute time step and a mean horizontal distance of 75 km of the trajectories that show that the

results of the run with the lower horizontal and time resolution are nearly identical.”. Changed the resolution of the ERA Interim data in the runs in section 4.1 and section 5 to  $0.75^\circ \times 0.75^\circ$ .

- **F) Figure 3 is not properly discussed: how is this profile applied in the extratropics? There it does not make much sense that convection can reach an altitude of 15 km . . . so the profile should be scaled with the local tropopause height.**

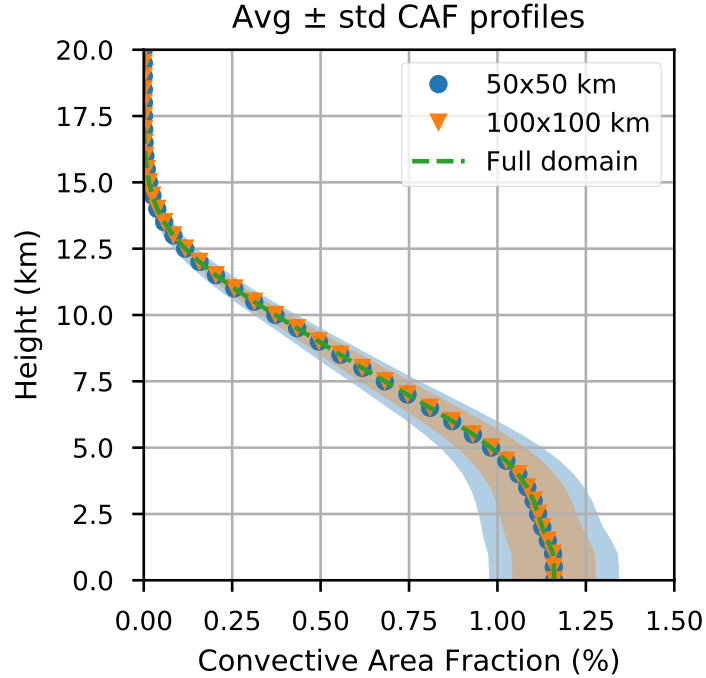
We agree that this was not clear. The scheme was originally developed for an application in the tropics (original manuscript page 8, line 21). Strictly speaking, an application of the algorithm in the extratropics would require a different convective area fraction profile. However, the global long-time simulations of radon are not sensitive to the choice of the convective area fraction profile because of the globally constant lifetime of radon (see explanation in reply to comment I). Hence, using a tropical profile in the radon runs does not noticeably change the results compared to a run using a profile for the mid-latitudes.

*Changes to the manuscript:* We added additional discussion along these lines in section 3.1 and a detailed explanation in new section 4.4.4 (see reply to major comment I).

**And the values for the convective area fraction, is it correct that they only make sense for a given grid size**

This is correct and we agree that it is important to discuss this in section 3.2. The frequency distribution of the measured convective area fractions depends on the domain size of the CPOL radar. The domain size should be comparable to the grid size of the meteorological analysis data to obtain a meaningful distribution of vertical updraft velocities. The full domain size of the radar is  $190 \times 190 \text{ km}^2$ , which is comparable to the horizontal resolution of  $2^\circ \times 2^\circ$  of the ERA Interim data. As the domain size decreases, the frequency distribution approximates a bimodal distribution: In the limit of domain sizes below typical cloud sizes, the fraction can only be 0 or 1. That is, grid cells completely covered by convection and completely free of convection become more frequent (e.g. Arakawa and Wu, J. Atmos. Sci., 70, 7, 1977-1992, 2013).

It is desirable that the method gives meaningful results for other resolutions than  $2^\circ \times 2^\circ$  and can be applied in the range of typical GCM and reanalysis resolutions. In fact, in response to the other reviewer, now also runs with  $0.75^\circ \times 0.75^\circ$  resolution are performed.



The figure shows the dependence of the standard deviation of the frequency distribution of measured convective area fractions on the used domain size of the CPOL radar. Results are shown for domain sizes of  $190 \times 190 \text{ km}^2$ ,  $100 \times 100 \text{ km}^2$  and  $50 \times 50 \text{ km}^2$ . For the smaller domain sizes, the measurement domain of the radar has been divided into smaller subdomains. It is evident that the frequency distributions for different domain sizes differ significantly.

The current implementation of the algorithm does not consider this effect, and it is not clear if incorporating a distribution of the convective area fractions which depends on the grid size would lead to a significant change of the results of trajectory runs or not. An implementation of frequency distributions of the convective area fraction that depend on grid size is only planned for a future version, since this would mean a considerable additional effort.

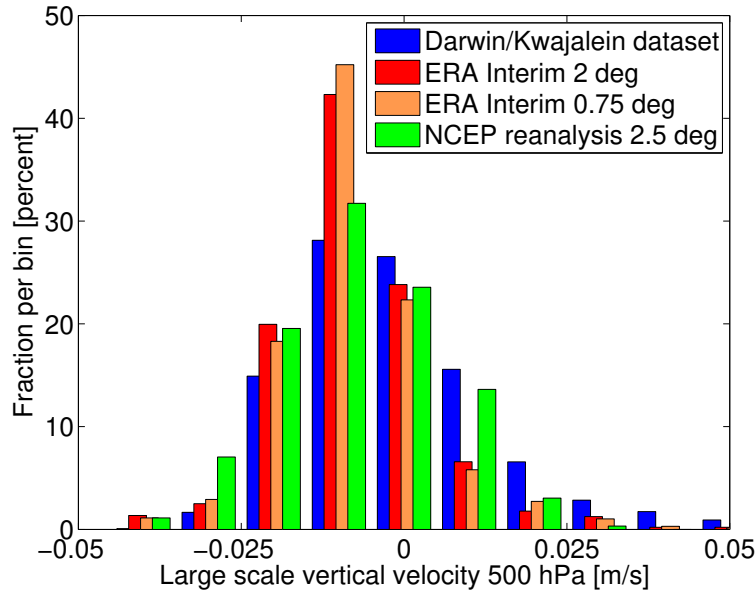
*Changes to the manuscript:* Added discussion to section 3.2 along the lines outlined above. Added figure of the standard deviations for different domain sizes.

- G) However, quantitatively the vertical velocity field is extremely sensitive to the choice of the reanalysis (e.g., NCEP vs. ECMWF) and even more so on the resolution (e.g., ERA-40 vs. ERA-

**Interim). Therefore — it seems to me — the frequency distribution must be recalculated each time data is used from a different model / reanalysis. Please discuss.**

This is a good point. It is important for the method that the large-scale vertical velocities from the Darwin/Kwajalein dataset and the large-scale velocities from the reanalysis used for the trajectory calculations have a similar distribution.

The figure shows the frequency distributions of the vertical velocity at 500 hPa from the Darwin dataset, ERA Interim and NCEP, and additionally, two different horizontal resolutions for ERA Interim ( $0.75^\circ \times 0.75^\circ$  and  $2^\circ \times 2^\circ$  resolution). For the reanalysis data, the vertical velocity at 500 hPa at all grid points between  $180^\circ$  E and  $240^\circ$  E and  $30^\circ$  S and  $30^\circ$  N for the arbitrary date 1 June 2010 is used. The frequency distribution of the large scale vertical velocities of the Darwin dataset compares sufficiently well with the frequency distribution of the reanalyses and differences are acceptable in view of other uncertainties of our method, e.g. the uncertainties of the convective area fraction.

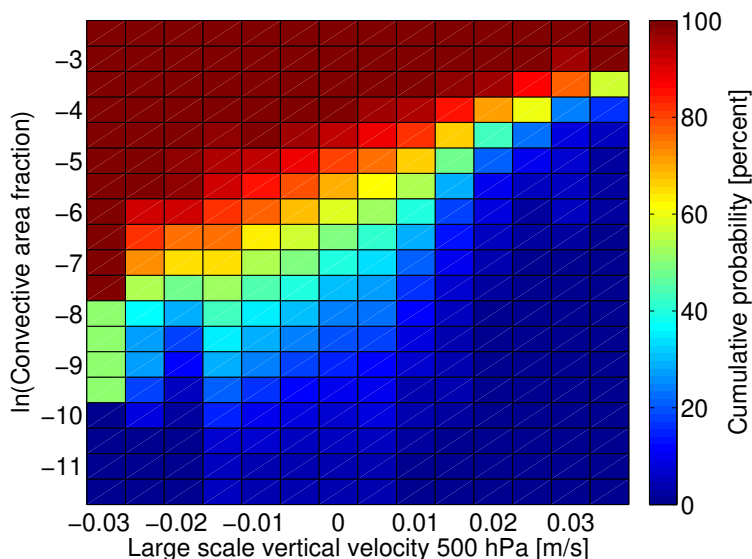


Hence, we did not apply a scaling or other correction to the large-scale vertical velocities from ERA Interim. But there may be cases where the vertical velocities from different reanalysis datasets have to be shifted or scaled to obtain a realistic distribution of the convective area fractions.

*Changes to the manuscript:* We added a paragraph and the figure above to section 3.2 and discuss the dependence of the method on the different distributions of the large-scale vertical velocity fields in the different reanalyses.

**The resulting lookup table is mentioned but nothing is shown.**

The figure shows the cumulative distribution of the convective area fraction as a function of the large scale vertical wind, which is used as the lookup table.



*Changes to the manuscript:* Added the figure showing the lookup table to the new manuscript.

- H) **Where simulation results are described and interpreted (e.g., p. 15 line 17), the paper is very brief. The reader would like to better understand the differences between the experiments.**

We expanded the discussion of the radon runs in section 4.4.4 (section 4.2 in original manuscript). We added that the runs with convection generally show higher radon concentrations than the runs without convection in the middle and upper troposphere due to the fast transport of radon from the boundary layer to the detrainment level. A more detailed interpretation of the profiles is however difficult due to the large-scale horizontal averaging.

We added additional discussion to section 4.4 (section 4.2 in the original manuscript) on how well the results of other studies compare to radon measurements to put the comparison of our model to radon measurements into perspective. Other studies show differences between their models and the radon measurements of a similar order of magnitude (see major comment B).

A discussion of the implications of the results of the SO<sub>2</sub> runs and of the scientific relevance of developing a convection model which simulates the time spent in updrafts was added: We added a discussion of the implications of the differences in the simulation of SO<sub>2</sub> in the different sensitivity

runs to section 5 and a paragraph discussing very-short lived bromine species to show that this is also relevant for other species than SO<sub>2</sub>.

*Changes to the manuscript:* Expanded the discussion of the radon runs in section 4.4.4. Added discussion to section 4.4 (section 4.2 in the original manuscript) on how well the results of other studies compare to radon measurements. Added discussion of the implications of the results of the SO<sub>2</sub> runs to section 5. Added a paragraph discussing very-short lived bromine species to section 5.

- **I) I must say that I don't understand the so-called "random CAF scheme". First, the description in Section 3.2 is not clear to me.**

Vertical updraft velocities are obtained from combining convective mass fluxes from meteorological analysis data with a parameterization of convective area fraction profiles. We implement two different parameterizations for the convective area fraction, a parameterization using an observed constant convective area fraction profile as well as a parameterization which uses randomly drawn profiles to allow for variability in the convective area fractions. We rephrased the abstract, introduction and conclusions to make that more clear and rephrased section 3.2 to provide a more detailed explanation.

Furthermore, we hope that the reply to comment F (dependence of convective area fraction on grid size) and comment G (dependence of large scale vertical velocity on reanalysis, figure showing lookup table) and the additional discussion in section 3.2 make it more clear what has been done.

*Changes to the manuscript:* Rephrased abstract, introduction, section 3.2 and conclusions along the lines outlined above.

**Then, from Figs. 13 and 14 it looks like "random CAF" differs quite a bit from "constant CAF", but when looking at the tracer experiments (Figs. 9–12, 15), then the two schemes yield almost identical results. Why is this the case?**

The reason for the almost identical results for the radon simulations is that the lifetime of radon is globally constant. For a tracer with a globally constant lifetime, it makes no differences if it was transported slowly upwards from the emission at the boundary layer to 10 km in the last 10 days or if it first was transported quickly by convection to 10 km within one hour, and then stayed at 10 km for 9 days and 23 hours. The amount of radon that decays only depends on the time passed since the last contact with the boundary layer, when it was emitted (see original manuscript page 15, lines 21–26 and new section 4.4.4).

Differences have to be expected for the SO<sub>2</sub>-like tracer. These differences are relatively small in our model runs, which means that the results are insensitive to the uncertainties in the parameterization of the vertical updraft velocities.

*Changes to the manuscript:* We added additional discussion of the effect of globally constant lifetimes along the lines outlined above to section 4.4.4.

**And why then should the reader and in general the CTM user community care about the difference between the two schemes?**

It is not implied in the text that the community should care about the difference. It is a valid approach to try out several approaches in a new algorithm and to see what works best or if several approaches yield similar results.

### Minor comments

- **page 1, line 15: this last sentence appears totally unrelated to the rest of the abstract. Include what the outcome is of this updraft velocity validation.**

The sentence was directly related to the preceding sentence, which mentioned the validation of the mass conservation and validation with radon.

*Changes to the manuscript:* We rephrased the abstract to include the main results of the validation.

- **page 1, line 18: "correct" – > "accurate" or "appropriate"**

*Changes to the manuscript:* Changed.

- **page 2, line 28: no need for future tense**

*Changes to the manuscript:* Changed.

- **page 3, line 14: "and" – > "times"**

*Changes to the manuscript:* Changed to "multiplied by".

- **page 3, line 31: How does the updraft dominate the downdraft mass flux? By intensity? Integrated over the domain, they must be very similar, given mass conservation.**

This is a misunderstanding caused by the confusion of the downdraft mass flux in the cloud with the slow subsidence outside of the cloud. The subsidence outside the clouds has to balance the convective mass flux inside the clouds (sum of updrafts and downdrafts), see section 2.6 (2.5 in the original manuscript).

*Changes to the manuscript:* We added the phrases "updraft inside clouds", "downdraft inside clouds" and "subsidence outside clouds" at some additional locations.

- **page 4 and 6: combine Figs. 1 and 2 as two panels in one Figure**

We would like to keep the separate figures. We do not see a benefit in combining the figures.

- **page 5, line 9: this sentence is awkward, please rephrase.**

*Changes to the manuscript:* Split up into two sentences: "If a parcel is marked as taking part in convection, it is transported upwards for the vertical distance that it will be able to ascend in one intermediate convective time step  $\Delta t_{\text{conv}}$  (10 seconds). The vertical distance is determined by the vertical convective updraft velocity."

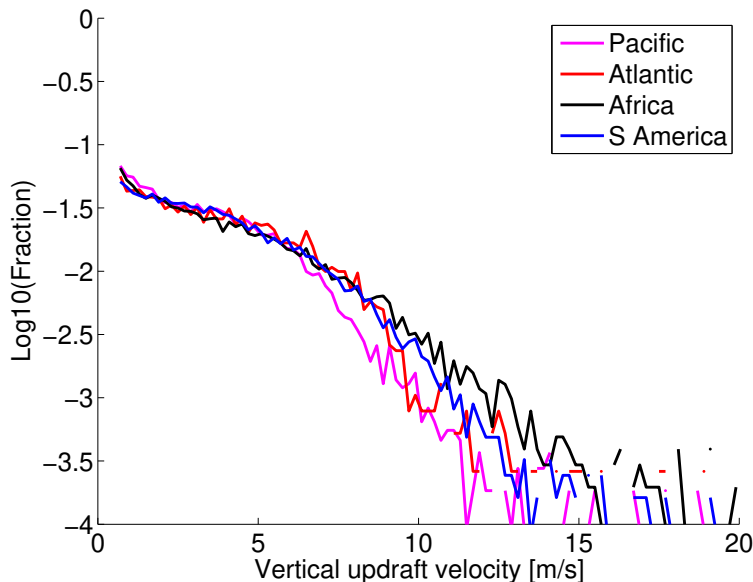
- **page 5, line 13: "m/s"  $\rightarrow$   $\text{m s}^{-1}$**

*Changes to the manuscript:* Changed throughout the manuscript.

- **page 6: why is section 2.4 not directly after 2.2?**

This is the natural temporal order of the events: 2.2 entrainment, 2.3 upward transport, 2.4 detrainment. This is also the order of the steps in the algorithm (see original manuscript page 3, lines 11–16).

- **page 10, line 7: I would be curious to see pdf of wu for different regions.**



The plot shows the pdf of the vertical updraft velocities derived from ERA Interim (model level 21, corresponding to about 520 hPa, June 2010) for four different regions: Pacific (180–240° E, 15° S–15° N), Atlantic (330–345° E, 15° S–15° N), Africa (0–45° E, 15° S–15° N), South America (285–315° E, 15° S–15° N). There are no significant differences for velocities below about 7 m/s. The percentage of velocities  $> 20$  m/s is lower than 0.1% for all regions.

- **page 11, line 3: "simplified and non-realistic"  $\rightarrow$  "idealized"**

*Changes to the manuscript:* Changed.

- **page 11: Figure 4 is not discussed at all.**

This is only intended as an example, and we feel that a short description is sufficient.

- **page 13: combine Figs. 6 and 7 as two panels in one Figure.**

See comment to page 4 and 6 above.

- **page 15: the order of the sections is somehow strange: 4.3 would be better after 4.1 and 4.2 and 4.4 are also somehow related.**

*Changes to the manuscript:* Changed as requested. Moved section 4.2 (original manuscript) to the end of section 4. Section 4.2 (original manuscript) is now section 4.4 (new manuscript), section 4.3 (original manuscript) is section 4.2 (new manuscript) and section 4.4 (original manuscript) is section 4.3 (new manuscript). Divided 4.4 into additional subsections.

- **page 16: combine Figs. 9-12 as four panels in one Figure.**

See comment to page 4 and 6 above.

- **page 20, line 3 and 13: sentences should not start with "i.e." or "e.g."**

*Changes to the manuscript:* Changed to "That is" and "For example", respectively.

- **page 20, line 2: why does the random CAF scheme lead to higher velocities? This is not clear to me.**

The fact that the vertical updraft velocities are typically larger when a randomly drawn convective area fraction profile is used can be readily understood qualitatively: Assuming that  $M$ ,  $T$  and  $p$  are fixed, the mean updraft velocity in case of a mean constant convective area fraction profile  $\langle f_{\text{up}} \rangle$  is simply  $\langle w_{\text{up1}} \rangle = \frac{MRT}{\langle f_{\text{up}} \rangle p}$ , where  $\langle \dots \rangle$  denotes the mean over all air parcels. In the case of a varying randomly drawn convective area fraction profile, the mean vertical updraft velocities need to be expressed as  $\langle w_{\text{up2}} \rangle = \langle \frac{MRT}{f_{\text{up}} p} \rangle = \frac{MRT}{p} \langle \frac{1}{f_{\text{up}}} \rangle$ . Since  $\langle \frac{1}{f_{\text{up}}} \rangle \geq \frac{1}{\langle f_{\text{up}} \rangle}$  due to the fact that the harmonic mean is always smaller than the geometric mean, we obtain the relation  $\langle w_{\text{up2}} \rangle \geq \langle w_{\text{up1}} \rangle$ . This implies that also individual realizations of  $w_{\text{up}}$  are on average larger for the random convective area fraction profiles.

*Changes to the manuscript:* Added discussion to section 4.2 (section 4.3 in the original manuscript) along the lines discussed above.

- **page 22: Figure 15 clearly shows the most relevant and interesting result of the paper. I understand that no observations are available to verify these profiles, but I think a more detailed discussion of these profiles is important. The differences are fairly large. What does this imply for tropospheric chemistry?**

We agree that a discussion of the implications of the results of the SO<sub>2</sub> runs and of the scientific relevance of developing a convection model which simulates the time spent in updrafts is important. We added a discussion of the implications of the differences in the simulation of SO<sub>2</sub> in the different sensitivity runs to section 5. In addition, we added a paragraph discussing very-short lived bromine species to show that this is also relevant for species other than SO<sub>2</sub>.

*Changes to the manuscript:* We extended the discussion in section 5 by adding paragraphs discussing the implications of the changes in the SO<sub>2</sub> simulations and a paragraph discussing very-short lived bromine species as an example for another species for which this could be relevant.

**How would the results look like if using a convective transport scheme as implemented in other CTMs...**

This is a question we are also interested in. We added discussion of how well the results of other models compare to radon measurements in section 4.4.4. A detailed comparison study of several convective transport models is outside the scope of this technical presentation of an algorithm. This would mean a considerable additional effort.

Differences between different models in other studies will often mainly be due to differences in the underlying convective parameterization (see e.g. Feng et al., 2011). This is however a very extensive and difficult topic (e.g. Arakawa, 2004), which is outside the scope of this study.

*Changes to the manuscript:* We added some discussion of how well the results of other models compare to radon measurements in section 4.4.4.

**... or in FLEXPART?**

FLEXPART does not provide single trajectories as output which one could use to run a box model. We are restricted to the build-in simplified chemistry schemes, which are an exponential decay with a fixed lifetime and a simple OH scheme (e.g. Pisso et al., Geosci. Model Dev., doi:10.5194/gmd-2018-333). Hence, it is not possible to do a meaningful comparison due to constraints in FLEXPART.

We thank the referee for taking the time for reading our manuscript and their helpful comments!

### General changes

- We have considerably changed the text throughout the manuscript to improve the logical order of the text and to improve the explanations and comprehensibility. We added new subsections and improved the use of the English language.

### General comments

- **Combined reply to the following:**
  - 2. From the work presented it becomes obvious that validation, and specifically the validation of the core component — the residence times during convective updrafts — is very difficult.**
  - 4. Admitting that the validation problem is largely inherent and not easily overcome, I think the paper could be acceptable if it would limit itself to a description of the algorithm implemented together with tests conducted so far, while including a clear characterisation of the limitations and the way how a more robust testing and/or tuning will be done, and making it at least plausible that the scheme will be superior to simpler alternatives.**

We agree that more discussion of these issues was needed. Currently, the large uncertainties in emissions, chemistry, microphysics and measurements of many short-lived species do not allow for a quantitative assessment whether our scheme improves the simulation of these short-lived species, even if this is suggested by the more realistic simulation of the time spent in convective clouds. Rather, our scheme allows for estimating the uncertainties in the simulation of these species associated with different parameterizations of vertical transport in convective updrafts. These uncertainties generally pose a challenge for the validation of the simulation of short-lived species, and there is a clear need to improve on this situation (as also noted by e.g. Forster et al., 2007).

In addition, the globally constant lifetime of radon does not allow to validate the parameterization of the time spent in convective updrafts. Nevertheless, currently radon is probably still the species most suitable for the validation of convective transport models, since there is a lack of good alternatives.

We have added discussion to section 4.4 on how well the results of other studies compare to radon measurements to put the comparison of our model to radon measurements into perspective. Other studies show differences between their models and the radon measurements of a similar order of magnitude (Jacob et al., 1997, Collins et al., 2002, Forster et al., 2007, Feng et al., 2011).

For many physical parameterizations in GCMs and CTMs there is no sufficient data for validation. The only way to make it more plausible that they are superior is to state that the physical assumptions are closer to reality.

*Changes to the manuscript:* We extended the discussion in the introduction and conclusions to discuss the large uncertainties in the validation of short-lived species as outlined above and to discuss the validation with radon. In addition, we added discussion in section 4.4.4 (section 4.2 in original manuscript) how well other models compare to the radon measurements and on the uncertainties in radon emissions, simulations and measurements.

- **2. The claim of the paper of a successful validation appears to be not sufficiently supported.**

We are aware that validation of the model is difficult and paid attention to a careful formulation of the results. The only occasion in the original manuscript, where we speak of an "successful validation" is at page 22, line 14 in the conclusions. This only refers to the technical part of the validation, i.e., mass conservation and reproduction of the convective mass fluxes and detrainment rates from the reanalysis. Since this part of the sentence is not really needed, we deleted it to avoid confusion.

*Changes to the manuscript:* Deleted "The algorithm is successfully validated by showing that" from the sentence.

- **3. The usefulness of the scheme in the context of the whole model will also depend on how well the chemical environment inside a convective cloud is actually modelled. The manuscript is not giving much attention to this aspect, which probably depends strongly on the model resolution (i.e. number of Lagrangian parcels). In addition, it should be compared to the option of just parameterising key reactions such as the heterogeneous oxidation in convective clouds.**

The chemistry scheme is a part of the model which is independent from the transport scheme, and we think that a discussion of chemistry schemes is better suited to a separate study, which may for example study the effects that the different model components have in a complete GCM or CTM.

This is a technical paper presenting a new algorithm for a convective transport scheme. While it is certainly very interesting and important, it is out of the scope of this study to perform a detailed comparison of complex chemistry schemes or to discuss the chemistry of short-lived species like SO<sub>2</sub> in detail.

This model was originally developed as part of a larger study of the chemistry and transport of SO<sub>2</sub> from the troposphere to the stratosphere. An important part of this study is how the numerous uncertainties in SO<sub>2</sub>

chemistry, convection, transport and microphysics translate into uncertainties in the SO<sub>2</sub> mixing ratios. It was decided to split the publication of this study into two papers. The combined study would have been too extensive and it is not a good idea to start a study about SO<sub>2</sub> with a long technical description of a convection model.

Unfortunately, a meaningful validation of the model is difficult with these SO<sub>2</sub> simulations and measurements. There are so many uncertainties that the results always can be tuned to agree with the measurements.

### Specific comments

- **1. It would be good to include a brief introduction to the ATLAS model and how it works, so that the paper can be understood well without first reading other papers, as there is no easy or natural method to include complex chemistry into a Lagrangian model.**

The ATLAS model is a model consisting of several independent modules. In this study, only the trajectory module is used. The chemistry module and the mixing module are not used.

Radon and SO<sub>2</sub>-like tracer mixing ratios are calculated with a simple exponential decay and fixed lifetimes. The more sophisticated chemistry model, which is implemented in the full ATLAS model and uses a system of coupled differential equations, is not employed.

*Changes to the manuscript:* We changed the text in several locations (abstract, introduction, section 4, conclusions) to make clear that only the trajectory module is used. Added that the trajectory module uses a 4th order Runge-Kutta scheme.

- **2. Page 4 L 1ff: These sentences are not sufficiently precise, for example, it is not possible to speak about the mass of a trajectory.**

It probably was not clear what the discussion was aiming at.

We agree that there is no natural way to assign a mass to a single trajectory air parcel. One could argue that a trajectory air parcel only refers to an infinitesimal volume and that only intensive quantities like density are well defined for an air parcel, while extensive quantities like mass are not well defined.

However, in a global model, where the model domain is filled with trajectory air parcels, this looks different. Here, the volume of the model domain can be divided into smaller subvolumes that make up the complete volume. Each subvolume can be associated with a trajectory air parcel, with the air parcel mass given by the product of density of air and air parcel volume. The same constant mass can be assigned to each trajectory air parcel, which implies that the associated volume is increasing with decreasing air density. Since the subvolumes should not overlap to

avoid that the same air volume is counted twice, this means that trajectory air parcels are distributed uniformly over pressure (but exponentially decreasing over altitude).

This is not merely a theoretical consideration, but becomes important when e.g. the global mass of a chemical species is calculated, or the mass flux of a chemical species through a control surface (as the tropopause).

*Changes to the manuscript:* We considerably extended the discussion in section 2.1 as outlined above and moved the discussion to a new subsection 2.2.

- **3. Figures 1 and 6: The blue colour does print well.**

You probably mean "does not print"? A darker blue is used now.

- **4. Page 5, Eq 4: The equation of state should contain moisture**

For a worst case scenario with a temperature of 300 K and a relative humidity of 100 %, the change in density compared to the dry density is 2.2 %. This is negligible given the uncertainties of the method.

*Changes to the manuscript:* We added a note to the text.

- **5. Page 5, Eq 5 ff. One would better use just  $c$  as subscript.**

Thanks for noting this. That was inconsistent throughout the manuscript, sometimes  $c$  was used, and sometimes "conv".

*Changes to the manuscript:* We changed the subscript to "conv" consistently (see also below).

- **6. Page 6 Eq. 7 ff: Better not to use (long) words as subscripts.**

In our opinion, short words as subscripts help to understand the equations. We agree that very long words (e.g. "subsidence") make the equations hard to read.

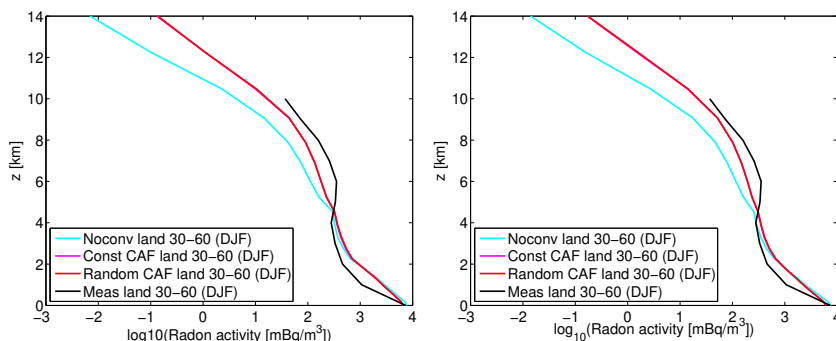
*Changes to the manuscript:* We changed all subscripts of all variables consistently to consist of short words.

- **7. Page 10, L 22: It is not clear why an artificially degraded resolution of 2 degrees is used for the meteorological input from ERA-Interim.**

The difference is due to computational constraints. The long-time run comprises more than 15 years. Simulation time is considerably reduced by changing the resolution from the original resolution of  $0.75^\circ \times 0.75^\circ$  to a resolution of  $2^\circ \times 2^\circ$  without changing the results significantly.

The results of the long-time runs are not particularly sensitive to the resolution of the reanalysis data. 1-year runs with a time step of 10 minutes,  $0.75^\circ \times 0.75^\circ$  resolution of the analysis and a mean distance of the trajectories of 75 km have been performed to demonstrate that the results do not change significantly (a related comment of reviewer 1 asked for the

difference that the change in time step from 10 min in the simplified run to 30 min in the radon run would cause). The runs with a time resolution of 30 min, a horizontal resolution of  $2^\circ \times 2^\circ$  and a mean distance of 150 km give nearly identical results (see figure, left:  $2^\circ \times 2^\circ$ , 30 min from Fig. 10 manuscript, right:  $0.75^\circ \times 0.75^\circ$ , 10 min).



The idealized runs from section 4.1 and the  $\text{SO}_2$  run, which comprises a shorter time period, are based on ERA Interim data with a resolution of  $0.75^\circ \times 0.75^\circ$  now.

*Changes to the manuscript:* We added discussion of the 1-year runs to section 4.4.1 (section 4.2 in original manuscript). We increased the resolution to  $0.75^\circ \times 0.75^\circ$  in the simplified runs in section 4.1 and for the  $\text{SO}_2$  runs in section 5.

- **8. Figure 4 and others: It would be good to frame figures (with tick marks on the upper and right axis)...**

*Changes to the manuscript:* Done.

**... and to use secondary ticks as appropriate (in Fig. 4, for each day).**

We are sorry that this is not feasible. Our software does only allow automatic placement of secondary tick marks, but there is no control over the spacing.

**The number of digits given should not vary along one axis.**

It is common practice that digits vary. For example, we do not think it makes sense to label the pressures "0800", "0900", "1000" or the mass flux "0.025", "0.030".

- **9. Page 14, L 10–11: I am wondering why trajectories were initialised at random positions rather than on an equal-area grid.**

The random positioning is the default for trajectory initialization in the ATLAS model. It is normally used to avoid that an initialization on a regular grid can have any systematic effect on the results. It was used here for simplicity. An equal-area grid would probably work equally well for the application in this study.

*Changes to the manuscript:* We added that this is the default initialization scheme of ATLAS and that it is normally used to avoid any systematic effects to the paragraph in section 4.4 (4.2 in original manuscript).

**Also, the 150 km horizontal resolution seems to be add odds with a random positioning.**

This indeed needs a better explanation.

*Changes to the manuscript:* We changed the text to "Trajectories are initialized at random positions (both horizontally and in pressure) between 1100 hPa and 50 hPa. The number of trajectories is chosen in such a way that the mean horizontal distance of the trajectories is 150 km in reference to a layer of a width of 50 hPa."

- **10. Page 14, L 28 ff: "Radon is distributed evenly over these parcels by assuming a well-mixed boundary layer" Wording is not good.**

*Changes to the manuscript:* Rephrased the sentence to "Radon is emitted into all trajectory air parcels that are in the boundary layer by assuming a well-mixed boundary layer, and a volume mixing ratio  $x$  of. . ."

**Eq. 13 is not an equation.**

*Changes to the manuscript:* Changed the text to "volume mixing ratio  $x$ " and the equation to  $x = \dots$

**The emission rate would better not be denoted by  $e$  in a context where thermodynamic variables appear, it might be confused with vapour pressure.**

The disadvantage of using a letter different from  $e$  is that the association with the starting letter of "emission" is lost, so this is a compromise.  $\varepsilon$  is already used for the entrainment probability in the text, and  $E$  is used for the entrainment rate.

**It is also interesting to learn at this place that parcels transport volume mixing ratios, whereas in other places it was said that they represent masses.**

This is no contradiction. The basic assumption behind the concept of an "air parcel" is that it contains the same set of atoms at any given time. It follows that the mixing ratio of a given species is conserved along a trajectory (given that no chemical reactions take place) and that the mass of air is conserved.

- **11. Page 14–15, para. starting with line 33: The argument is not very clear. It would appear that an artificial minimum boundary-layer height of 500 m would systematically overestimate the input of  $R_n$  into the free atmosphere over land during winter, where probably the emission is already overestimated because of the snow cover effects.**

Our approach may cause some Radon which would be "trapped" in the boundary layer to end up in the free troposphere in the simulation and may cause some differences of the simulation to the Radon measurements.

However, assuming a minimum boundary layer height (or some similar measure) is unavoidable in global trajectory models, since the required number of trajectories needed for a model run which resolves the boundary layer by far exceeds any reasonable number that is computationally feasible.

The mass of radon emitted into the boundary layer per time period and area is still the same as with the actual boundary layer height and is not overestimated. This is accomplished by dividing by the boundary layer height  $z_{BL}$  in Equation 13.

*Changes to the manuscript:* We added discussion to the paragraph along the lines outlined above.

- **12. Page 15 L 17: I would not call this agreement "reasonable". Especially in Fig. 11 it is not good.**

We agree that a better explanation is needed why the agreement is called "reasonable, given the large uncertainties in measurements and emissions". We think that there are good reasons to keep this formulation.

We have now added discussion to section 4.4 (section 4.2 in the original manuscript) on how well the results of other studies compare to radon measurements to put the comparison of our model to radon measurements into perspective. Other studies show differences between their models and the radon measurements of a similar order of magnitude (e.g. Mahowald et al., 1995, Jacob et al., 1997, Collins et al., 2002, Forster et al., 2007, Feng et al., 2011). This suggests that a better agreement cannot be expected, given the uncertainties in measurement, emission and the simulation. The wording in other studies describing the agreement is comparable. E.g. Feng et al. states that their results "agree reasonably well" to the radon measurements. Their Figs. 13 and 14 show that the differences are comparable. Currently radon is probably still the species most suitable for the validation of convective transport models, since there is a lack of good alternatives.

The underestimation of radon by the simulation in Fig. 11 has also been observed in other studies (e.g. Jacob et al., 1997, Forster et al., 2007). This may be due to uncertainties in emission and due to the fact that measurements from coastal areas are included, where horizontal radon gradients are high and difficult to model (see Forster et al., 2007).

*Changes to the manuscript:* We extended the discussion as outlined above. Discussion was added to the introduction and conclusions, discussion in section 4.4 (4.2 in the original manuscript) was extended, and a discussion of the differences seen in Fig. 11 was added.

**One is also wondering why no comparisons with single flights were done in the 1990ies there are ERA-Interim data.**

The uncertainties of both the simulation and the radon measurements are so large that the data need to be averaged to obtain meaningful results. This is the common approach in most studies (e.g. Forster et al., 2007, Feng et al., 2011).

- **13. Page 16, Figure 8: It is not clear what "Points per layer" means.**

*Changes to the manuscript:* Changed to "trajectory air parcels per layer".

- **14. Page 16 ff, Figures 9-12: It would be more instructive to show mixing ratios rather than concentrations.**

The plots show the frequency of radioactive decay events (mBq) per volume ( $\text{m}^3$ ), which is proportional to concentrations. This is the standard unit for radon, which is found in the majority of the publications (see e.g. Mahowald et al., 1995, Collins et al., 2002, Feng et al., 2011). For the reason of being comparable to other studies, we would like to stick to the units.

- **15. Page 18 L 9 ff: Do not repeat explanation of the colour of curves in the text.**

We do not see a disadvantage. We would like to keep the text as is.

- **16. Page 18 ff, Section 4.3: The implications of choosing a specific cut-off value for the vertical velocity need to be discussed.**

We substantially extended and rephrased this discussion. Part of the problem is caused by the conceptual problem of defining what a convective updraft is in the measurements. It is common to apply a lower threshold to the vertical updraft velocities to define convective situations in the measurements. Typically, this threshold is between  $0 \text{ m s}^{-1}$  and  $1.5 \text{ m s}^{-1}$  and may have a significant effect on the results (e.g. Kumar et al., 2015). Note that the  $0.6 \text{ m/s}$  cut-off is applied in Fig. 15 only for comparison. It does not appear in the model formulation.

Replacing the simulated vertical updraft velocities by the measured vertical updraft velocities in the model would increase the average residence time between entrainment and detrainment. In turn, this would lead to a lower concentration of a short-lived species like  $\text{SO}_2$  in the upper troposphere.

*Changes to the manuscript:* Substantially expanded and rephrased the discussion in section 4.2 (4.3 in the original manuscript) as outlined above.

**Would it help to use cumulative frequency distributions rather than probability densities?**

No. Since the cumulative frequency distribution is the integral of the probability density, changes at the small values of velocity will affect the values of the cumulative frequency distribution at large velocities.

- **17. Page 21, Figure 14: A step function or just symbols should be used, not continuous curves, as the data represent binned values.**

In this case the binned data is used to approximate a curve which should be continuous in theory (by using an infinite number of bins). For this plot, which shows 30 bins, there is hardly any difference to a "continuous" curve.

- **18. Page 22, L 15–16: The Rn simulation is not suitable to demonstrate the proper long-term stability of mass distribution as radon has a short lifetime.**

This is a misunderstanding. Radon is not used to demonstrate the long-term stability of the mass distribution. The long-term run is used for two separate purposes: a) To demonstrate the stability of the mass distribution, and b) to validate the model with radon. The radon mixing ratios are not needed to demonstrate the stability of the mass distribution, and the positions of the trajectories are sufficient for this. The stability of the mass distribution is demonstrated by counting the trajectory air parcels in a given altitude layer. Since every trajectory parcel is associated with a constant mass, this is equivalent to determining the mass in a layer.

*Changes to the manuscript:* Changed the text in several locations to avoid misunderstandings: Added a new section 4.4.3 with the title "Conservation of vertical mass distribution". We changed the text in section 4.4.3 (originally section 4.2, page 14, lines 19–24) by including: "We revisit the issue of the conservation of the vertical mass distribution in this more realistic setup (compared to the idealized setup in Section 4.1)". We changed "mass distribution" in the sentence "The number of trajectories . . . at the start . . . compares well with the mass distribution at the end" to "number of trajectories". Added "conservation of vertical mass distribution of air (not of radon)" to the description in the text.

- **19. a) Authors should pay more attention to upper vs. lower case.**

*Changes to the manuscript:* Changed.

- **b) Page 2 L 2: It is surprising to see species in a CTM called "tracers"**

*Changes to the manuscript:* Changed "tracers" to "species".

- **20. Code and data accessibility**

We would be happy to provide the source code to you by creating an account on our repository for you, if you feel this is necessary.

As far as we understand it from the "model and data policy" statement, we are obliged to make the source code available to the editor, so that would have been the designated point of contact to our understanding.

**It would also be nice if authors make available the old measurement data on-line in digital form (in which they must have them already), if it is legally possible, rather than pointing to printed publications.**

We have no permission to do that.

# A Lagrangian convective transport scheme including a simulation of the time air parcels spend in updrafts

Ingo Wohltmann<sup>1</sup>, Ralph Lehmann<sup>1</sup>, Georg A. Gottwald<sup>2</sup>, Karsten Peters<sup>3,\*</sup>, Alain Protat<sup>4</sup>, Valentin Louf<sup>5</sup>, Christopher Williams<sup>6</sup>, Wuhu Feng<sup>7</sup>, and Markus Rex<sup>1</sup>

<sup>1</sup>Alfred Wegener Institute for Polar and Marine Research, Potsdam, Germany

<sup>2</sup>School of Mathematics and Statistics, University of Sydney, New South Wales, Australia

<sup>3</sup>Max Planck Institute for Meteorology, Hamburg, Germany

<sup>4</sup>Bureau of Meteorology, Melbourne, Australia

<sup>5</sup>Monash University, Clayton, Australia

<sup>6</sup>NOAA, Boulder, Colorado, USA

<sup>7</sup>National Centre for Atmospheric Science, School of Earth and Environment, University of Leeds, Leeds LS2 9JT, UK

\* now at Deutsches Klimarechenzentrum GmbH (DKRZ), Hamburg, Germany

**Correspondence:** I. Wohltmann (ingo.wohltmann@awi.de)

**Abstract.** We present a Lagrangian convective transport scheme developed for ~~Chemistry and Transport Models and ensemble trajectory simulations. Similar to existing schemes in other Lagrangian models, it is based on a statistical approach of calculating parcel displacements by convection. These schemes redistribute air parcels within a fixed time step by calculating probabilities for entrainment and the altitude of detrainment. Our scheme extends this approach by modelling vertical updraft~~ velocities and the global chemistry and transport models, which considers the variable residence time that an air parcel spends inside the convective event, which is important for in convection. This is particularly important for accurately simulating the tropospheric chemistry of short-lived species, e.g. ~~it determines~~ for determining the time available for heterogeneous chemical processes on the surface of cloud droplets. ~~Two different schemes for determining the~~

In current Lagrangian convective transport schemes air parcels are stochastically redistributed within a fixed time step according to estimated probabilities for convective entrainment as well as the altitude of detrainment. We introduce a new scheme which extends this approach by modelling the variable time that an air parcel spends in convection by estimating vertical updraft velocities ~~are introduced, which are based on constant or random.~~ Vertical updraft velocities are obtained by combining convective mass fluxes from meteorological analysis data with a parameterization of convective area fraction profiles, respectively. SO<sub>2</sub> is used as an example to show that there is a significant effect on species mixing ratios when ~~modelling the time spent in convective updrafts compared to a nearly instantaneous redistribution of air parcels. The~~ We implement two different parameterizations, a parameterization using an observed constant convective area fraction profile as well as a parameterization which uses randomly drawn profiles to allow for variability. Our scheme is driven by convective mass fluxes and detrainment rates that originate from an external convective parameterization, which can be obtained from meteorological analysis data or ~~General Circulation Models. Validation runs from general circulation models.~~

We study the effect of allowing for a variable time that an air parcel spends in convection by performing simulations, where our scheme is implemented into the trajectory module of the ATLAS chemistry and transport model, and is driven by ECMWF

ERA Interim reanalysis data ~~are performed with the scheme implemented into the ATLAS Chemistry and Transport Model.~~ ~~These include long-term global trajectory simulations of Radon-222 that are compared to measurements, and runs testing mass conservation and the reproduction of.~~ In particular, we show that the redistribution of air parcels in our scheme conserves the vertical mass distribution and that the scheme is able to reproduce the convective mass fluxes and detrainment rates of ERA Interim. ~~Simulated~~ We further show that the estimated vertical updraft velocities ~~are validated by~~ of our scheme are able to reproduce wind profiler measurements ~~in Darwin.~~ performed in Darwin, Australia, for velocities larger than  $0.6 \text{ m s}^{-1}$ .

$\text{SO}_2$  is used as an example to show that there is a significant effect on species mixing ratios when modelling the time spent in convective updrafts compared to a redistribution of air parcels in a fixed time step. Furthermore, we perform long-time global trajectory simulations of radon-222 and compare with aircraft measurements of radon activity.

## 1 Introduction

The parameterization of sub-grid scale cumulus convection and the associated vertical transport is ~~not only a key process in General Circulation Models (e.g. Arakawa, 2004), but the correct~~ a key procedure in general circulation models (e.g. Emanuel, 1994; Arakawa, 2004) as well as in chemistry and transport models (e.g. Mahowald et al., 1995). In particular, an accurate simulation of convective transport is ~~also~~ important for the modelling of ~~tracers in Chemistry and Transport Models, and the treatment of convection is a large source of uncertainty for species in chemistry and transport models and would allow for a reduction of uncertainty in~~ the simulation of these species in the troposphere (e.g. Mahowald et al., 1995; Hoyle et al., 2011; Feng et al., 2011) (e.g. Mahowald et al., 1995; Forster et al., 2007; Hoyle et al., 2011; Feng et al., 2011).

Lagrangian (trajectory-based) models have several advantages over Eulerian (grid-based) models, for example they do not introduce artificial numerical diffusion and there is no additional computational cost for transporting more than one tracer species (e.g. Wohltmann and Rex, 2009).

We present a Lagrangian convective transport scheme developed for ~~Chemistry and Transport Models and ensemble trajectory simulations~~ global chemistry and transport models. The scheme can also be used for applications such as backward trajectories starting along flight paths or sonde ascents, where it allows for simulating the effect of convection when using a statistical ensemble of trajectories starting at every measurement location. Our convective transport scheme is based on a statistical approach similar to ~~the~~ schemes in other Lagrangian models (e.g. Collins et al., 2002; Forster et al., 2007; Rossi et al., 2016). ~~These schemes redistribute air parcels~~ In these schemes air parcels are redistributed vertically within a short fixed time step to simulate the effect of convection ~~and~~. The schemes are driven by convective mass fluxes and detrainment rates derived from a physical parameterization of convection. Typically, the time period between entrainment and detrainment is assumed to be fixed in these schemes, and varies between 15 minutes and 30 minutes in Collins et al. (2002), Forster et al. (2007) and Rossi et al. (2016). The fixed convective time step is not necessarily the same as the advection time step.

However, these schemes ~~These schemes therefore~~ do not take into account the different variable residence times of air parcels inside ~~the~~ a convective cloud. The amount of time spent inside the cloud is ~~important for calculations of~~ particularly important

55 when considering the tropospheric chemistry of short-lived species. The concentrations of these species in the upper troposphere may crucially depend on the transport time of an air parcel from the boundary layer to the upper troposphere (e.g. Hoyle et al., 2011). ~~Therefore, we extend the approach of earlier schemes by simulating the time air parcels spend inside a convective cloud.~~ An example for a species for which ~~that this~~ is relevant is the short-lived species SO<sub>2</sub>, which is depleted by a range of fast heterogeneous reactions inside clouds and by a gas-phase reaction with OH (e.g. Berglen et al., 2004; Tsai et al., 2010). ~~We perform runs with~~ (e.g. Berglen et al., 2004; Tsai et al., 2010; Rollins et al., 2017).

Therefore, we extend the approach of earlier schemes by simulating the variable residence time air parcels spend inside a convective cloud by estimating vertical updraft velocities. Vertical updraft velocities are obtained from combining convective mass fluxes from meteorological analysis data with a parameterization of convective area fraction profiles. The scheme is implemented into the trajectory module of the ATLAS chemistry and transport model (e.g. Wohltmann and Rex, 2009) and simulations are performed which are driven by ECMWF ERA Interim reanalysis data (Dee et al., 2011).

We test the scheme for the conservation of the vertical mass distribution and for reproducing the convective mass fluxes and detrainment rates of the meteorological analysis used for driving the model. Particular emphasis is given to the study of different methods of parameterizing the convective area fraction profiles needed to simulate vertical updraft velocities. All of these tests are performed with idealized trajectory simulations which ignore the large-scale wind fields to facilitate interpretation.

70 In addition, global long-time trajectory simulations which use the large-scale wind fields are performed. These include simulations of radon-222 which are compared to aircraft measurements and the simulation of an artificial tracer that is designed to imitate the most important characteristics of SO<sub>2</sub> chemistry ~~to show that there is a significant effect on tracer mixing ratios when using our scheme.~~

Radon-222 is widely used to validate convection models and to evaluate tracer transport (e.g. Feichter and Crutzen, 1990; Mahowald et al., 1995; Jacob et al., 1997; Forster et al., 2007; Feng et al., 2011). Radon is removed entirely by radioactive decay, and hence, no uncertainties in chemistry, microphysics or deposition have to be considered. Furthermore, the half-life time of 3.8 days is in the right order of magnitude to detect changes by transport on short time scales. However, meaningful conclusions from the validation runs are limited due to uncertainties in radon emissions and the relatively sparse coverage of radon measurements. In addition, the globally constant lifetime of radon prevents a validation of the parameterization of the time spent in convective updrafts, which would only be possible with a varying lifetime.

80 When considering convective transport of a SO<sub>2</sub>-like tracer in a global simulation we see a significant impact of the variable residence time on mixing ratio profiles, compared to a scheme with a ~~nearly instantaneous redistribution~~ redistribution of air parcels in a fixed time step.

The scheme is implemented into the ATLAS Chemistry and Transport Model (e.g. Wohltmann and Rex, 2009) and runs driven by ECMWF ERA Interim reanalysis data (Dee et al., 2011) are performed. outline of the paper is as follows: Section 2 and Section 3 describe the convective transport scheme and the corresponding algorithm. Section 2 describes the modelling of entrainment, upward transport, detrainment ~~and subsidence, and subsidence outside of clouds.~~ Section 3 describes the method to calculate vertical updraft velocities. In Section 4, ~~the scheme is validated. Mass conservation and performance of our scheme is tested.~~ The conservation of the vertical mass distribution and the reproduction of the mass fluxes and detrainment rates

90 from meteorological ~~data are tested, global trajectory-based simulations of Radon-222 analysis data are examined, global trajectory-based simulations of radon-222~~ are compared to measurements, and simulated vertical updraft velocities are compared ~~statistically~~ with wind profiler measurements from Darwin, Australia. In Section 5, simulations ~~with of~~ a SO<sub>2</sub>-like tracer are shown to demonstrate that using the scheme can have a significant effect on tracer mixing ratios. ~~We conclude with a discussion and summary in~~ Section 6 ~~contains the conclusions.~~

## 95 2 Description of the convective transport scheme

### 2.1 General concept

~~First, we will~~ We first present the algorithm for forward trajectories, and ~~will~~ introduce the necessary adaptations for backward trajectories at the end to facilitate understanding.

A statistical approach is taken, where entrainment and detrainment probabilities are calculated for each trajectory at every  
100 time step. Whether a given trajectory air parcel is entrained into ~~the a~~ cloud or detrained from ~~the a~~ cloud is then determined by drawing random numbers. The model is driven by convective mass fluxes and detrainment rates ~~from meteorological data or General Circulation Models and thus relies on an external convective parameterization. Since a~~ provided by meteorological analysis data or by general circulation models. Typical resolutions of meteorological analysis data are of the order of 1° x 1°. A grid box of the ~~meteorological~~ analysis typically contains several convective systems ~~that only cover~~ which only affect a  
105 small fraction of the mass contained in the grid box, which necessitates a statistical approach ~~is necessary.~~

~~The~~ We extend the approach used in existing convective transport schemes ~~is extended here by simulating the~~ by allowing for a variable time that an air parcel spends inside the convective event. ~~For this~~ To determine this time, vertical updraft velocities are calculated ~~from the meteorological analysis and some additional assumptions by combining convective mass fluxes from meteorological analysis data with parameterizations of convective area fraction profiles~~ (a detailed account is given in Sec-  
110 tion 3). Instead of calculating the probability that an entrained air parcel detrains at a certain altitude and then redistributing the parcels accordingly in a fixed time step (as in the ~~conventional approach~~), ~~a trajectory time step approach of Collins et al., 2002, or Forster et al., 2007), an advection time step of the trajectory model~~ is divided into smaller intermediate time steps convective time steps of a few seconds, and the parcel is moved upwards and tested for detrainment in each intermediate convective time step.

115 Our algorithm executes the following steps for each trajectory air parcel in every ~~trajectory advection~~ time step  $\Delta t$  ~~of the trajectory model~~ (typically 10 minutes):

1. Entrainment if air parcel is not in convection and if a test for entrainment is successful (Section 2.3)
2. If the air parcel ~~is takes part~~ in convection, the following two steps are repeated with a smaller intermediate convective time step  $\Delta t_c$   ~~$\Delta t_{conv}$~~  of 10 seconds until the air parcel detrains or the end of the present ~~trajectory time step (advection time step of the trajectory model  $\Delta t$ )~~ is reached:  
120

- Upward transport by the distance given by the convective time step ~~and  $\Delta t_{\text{conv}}$  multiplied by~~ the vertical updraft velocity (Section 2.4)
- Detrainment if a test for detrainment is successful (Section 2.5)

### 3. Subsidence of air parcels outside of convection in the environment (Section 2.6)

125 The ~~trajectory time step~~ advection time step of the trajectory model  $\Delta t$  needs to be sufficiently short for the algorithm to work (see Sections 2.3 and 2.5).

The Lagrangian convective transport model is driven by convective mass fluxes and detrainment rates from meteorological analysis data or from general circulation models and thus relies on an external convective parameterization. The convective mass flux  $M(z)$  at a given location, geometric altitude  $z$  and time in units of mass transported per area and per time interval is  
 130 related to the entrainment rate  $E(z)$  and the detrainment rate  $D(z)$  by mass conservation

$$\frac{dM}{dz} = E - D \quad (1)$$

where  $E$  and  $D$  are given in units of mass per area, per time interval and per vertical distance. ~~We define both~~ Both  $E$  and  $D$  are defined as positive numbers.

In ~~the meteorological~~ meteorological analysis data, the atmosphere is divided into several model layers. Usually, the convective mass flux is given at the layer interfaces, while the detrainment rates are given as ~~mean values per layer~~ the mean values of the layers. Entrainment rates can be calculated from the mass fluxes and detrainment rates by using Equation 1. In addition, the atmosphere is divided into grid boxes with a given horizontal resolution ~~in the meteorological analysis~~. In the ERA Interim meteorological ~~analysis~~ reanalysis,  $M$  is given as the ~~grid box~~ grid box mean convective updraft mass flux and  $D$  as the ~~grid box~~ grid box mean updraft detrainment rate per geometric altitude. The convective mass flux  $M$  is related to the mean convective  
 140 mass flux in the convective updrafts  $M_u$   ~~$M_{\text{up}}$~~  (per area of updraft) by

$$M = f_{\text{up}} M_u \quad (2)$$

where  $f_{\text{up}}$  is the convective area fraction, which is the fraction of the area of the grid box covered by updrafts in convective clouds. We will only consider updrafts here, since updraft mass fluxes typically dominate over downdraft mass fluxes in the clouds (see e.g. Figure 3 in Kumar et al., 2015, or Collins et al., 2002). It is planned to simulate downdraft mass fluxes in a  
 145 future version of the model.

## 2.2 The mass of trajectory air parcels

In the following, it is assumed that ~~the mass every trajectory air parcel is~~ associated with a ~~trajectory mass, which~~ is equal to the mass of the other ~~trajectories and remains constant~~. ~~This implies that for global model runs, the trajectories need to be distributed uniformly over pressure. The mass associated with the trajectory is then given by air density at the trajectory location and the volume it occupies.~~ trajectory air parcels and is constant in time. While there is no natural way to assign a mass to a single trajectory air parcel, this is different in a global model, where the model domain is filled with trajectory air  
 150

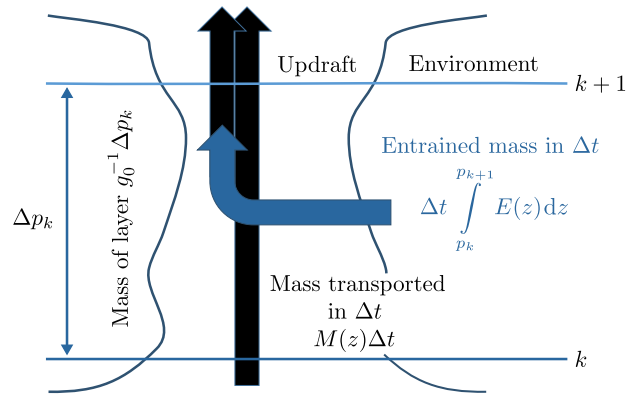


**Figure 1.** Schematic representation of the entrainment step. All quantities are per unit area.

parcels. One could argue that an air parcel only refers to an infinitesimally small volume and that only intensive quantities such as density are well defined for a trajectory air parcel, while extensive quantities such as mass are not well defined. However, in a global model, the volume of the model domain can be divided into smaller subvolumes that make up the complete volume. Each subvolume can be associated with a trajectory air parcel, and the air parcel mass is given as the product of the density of air and the air parcel volume. The same constant mass can be assigned to each trajectory air parcel, which implies that the associated volume is increasing with decreasing air density. Since the subvolumes of air parcels should not overlap to avoid that the same air volume is counted twice, this implies that the trajectory air parcels need to be distributed uniformly over pressure (but exponentially decreasing over altitude).

This is not merely a theoretical consideration, but becomes important when e.g. the total mass of a chemical species is calculated, or the mass flux of a chemical species through a control surface (as the tropopause).

The mass of a trajectory air parcel in such a model is typically much larger than the mass transported in a single convective event (e.g. Collins et al., 2002). For this reason and due to the statistical nature of the approach, results will only be meaningful if a sufficiently large ensemble of trajectories is examined before interpreting the results. The equations of the scheme are independent of the mass associated with the trajectory. Thus, in a global model where trajectory air parcels fill the model domain, a larger mass associated with a trajectory parcel (i.e. particular trajectory air parcel corresponding to a lower density of trajectory parcels per volume) leads to a lower number of trajectory air parcels in convection at a given point in time, which balances the higher mass moved per convective event.

### 2.3 Entrainment

For modelling the entrainment of the trajectory air parcels we follow the approach of Collins et al. (2002) and Forster et al. (2007) and assume that the atmosphere is divided into several layers, where layer  $k$  is confined by levels  $k$  and  $k+1$ , see as illustrated in Figure 1. These layers may be identified with the model layers of the meteorological analysis. For an air parcel located in a layer between pressures  $p_k$  and  $p_{k+1}$ , the probability  $\varepsilon$  of it being

entrained in a trajectory an advection time step of the trajectory model  $\Delta t$  is defined by the ratio of the mass per area entrained in a layer in a time step  $\Delta t$  and the mass per area of the layer. The entrainment probability is independent of the area covered by convection and is given by

$$\varepsilon = \frac{g_0 \Delta t \int_{z(p_k)}^{z(p_{k+1})} E dz}{\Delta p_k} \quad \text{with} \quad \Delta p_k = p_k - p_{k+1} \quad (3)$$

where  $g_0$  is the gravitational acceleration of the Earth and  $\int E dz$  is the grid-box mean entrainment rate integrated over the layer (resulting in the same units as the convective mass flux). The integration has to be performed over geometric altitude, which requires a conversion between pressure and geometric altitude. The equation is derived by dividing the mass per area entrained in a layer in a time step  $\Delta t$  by the mass per area of the layer. It is independent of the area covered by convection.

Whether an air parcel is entrained and takes part in convection is decided by generating a uniformly distributed random number  $r_e r_{\text{entr}}$  in the interval  $[0, 1]$  in every trajectory time step and comparing that to the calculated probability. If the random number is smaller than the entrainment probability  $r_e r_{\text{entr}} < \varepsilon$ , the air parcel is marked as taking part in convection and is therefore not tested for being entrained as long as it stays in convection. The trajectory time step advection time step of the trajectory model  $\Delta t$  needs to be sufficiently short for the algorithm to work to avoid that  $\varepsilon > 1$  (which would mean that the air in the layer would be ventilated several times by convection during the time step advection time step  $\Delta t$ ).

The time when the convective event starts of the entrainment event can be anywhere in the time interval between  $t$  and  $t + \Delta t$ . For simplicity, we assume that the convective event always starts at time  $t$ . This only results in a small shift of the convective event by a few minutes at most (depending on the model advection time step), which will be negligible in most cases.

## 2.4 Upward transport

If a parcel is marked as taking part in convection, it is transported upwards for the vertical distance that it will be able to ascend according to the vertical convective updraft velocity in one intermediate convective time step  $\Delta t_c \Delta t_{\text{conv}}$  (10 seconds). Then, it will be tested for detrainment (see Section 2.5). This procedure will be repeated until either the test for detrainment is successful or the end of the present trajectory time step advection time step of the trajectory model  $t + \Delta t$  is reached. The short intermediate time step convective time step  $\Delta t_{\text{conv}}$  is necessary to capture the steep vertical gradients in the detrainment rates and convective mass fluxes. For a strong updraft of  $10 \text{ m s}^{-1}$ , a time step of 10 s corresponds to a vertical distance of 100 m, which is usually sufficient to resolve the vertical levels of the analyses.

The vertical updraft velocity inside the convective cloud is given by

$$w_u = \frac{MRT}{f_u p}$$

where  $R = 287 \text{ J/kg/K}$  is the specific gas constant of air,  $T$  is temperature and the quantities are interpolated to the position of the air parcel. The equation is derived determined by noting that the convective mass flux in the cloud is the product of density and the vertical updraft velocity  $M_u = \rho w_u$  (with  $M_{\text{up}} = \rho w_{\text{up}}$ , where the density is given by  $\rho = p/(RT)$ ) according to the

205 ideal gas law), and by using  $R = 287 \text{ J kg}^{-1} \text{ K}^{-1}$  is the specific gas constant of dry air (neglecting modifications of  $R$  due to water vapour) and  $T$  is temperature. Using Equation 2, the resulting velocity is the vertical updraft velocity inside the convective cloud (in units of geometric altitude per time) is given by

$$w_{\text{up}} = \frac{MRT}{f_{\text{up}} p} \quad (4)$$

All quantities are interpolated to the position of the air parcel.

210 Neither convective area fractions  $f_u - f_{\text{up}}$  nor vertical updraft velocities  $w_u - w_{\text{up}}$  are usually available from meteorological analysis data. The approach used to overcome this problem in our convection scheme is to estimate a profile of  $f_u$  - we estimate profiles of the convective area fraction  $f_{\text{up}}$  based on observations. We implement two methods here: The first method uses an observed constant climatological convective area fraction profile, while the second uses a stochastic parameterization for randomly drawn convective area fraction profiles (Gottwald et al., 2016). A detailed discussion of the calculation of the vertical updraft velocities is given in Section 3.

215 The Once the vertical updraft velocity  $w_{\text{up}}$  is determined, the vertical geometric distance  $\Delta z_{\text{conv}} - \Delta z_{\text{conv}}$  that the air parcel ascends in an intermediate time step is convective time step  $\Delta t_{\text{conv}}$  is given by

$$\Delta z_{\text{conv}} = w_{\text{up}} \Delta t_{\text{conv}} \quad (5)$$

220 Under the assumption that the coordinate system of the trajectory model is log-pressure height  $Z$ , the distance that the parcel ascends in log-pressure height is

$$\Delta Z_{\text{conv}} = \Delta z_{\text{conv}} \frac{T_0}{T} \quad (6)$$

where log-pressure height is defined as  $Z = -H \log(p/p_0)$  and  $H = RT_0/g_0$ .  $T_0$  and  $p_0$  are the reference temperature and reference pressure of the log-pressure coordinate. Other coordinate systems will require equivalent transformations.  $\Delta Z_{\text{conv}}$  is added to the The new vertical location of a trajectory air parcel is determined by adding  $\Delta Z_{\text{conv}}$  to the initial vertical position of the parcel. Longitude and latitude are left The longitude and latitude of the parcel remain unchanged.

## 2.5 Detrainment

If a parcel is marked as taking part in convection and has been transported upwards, it is tested next for detrainment.

The probability that a parcel is detrained during an intermediate convective time step is

$$\delta = \frac{\int_{z_{\text{start}}}^{z_{\text{start}} + \Delta z_{\text{conv}}} D \, dz}{M_{\text{start}} + \int_{z_{\text{start}}}^{z_{\text{start}} + \Delta z_{\text{conv}}} E \, dz}$$

230 or, equivalently

$$\delta = \frac{\int_{z_{\text{start}}}^{z_{\text{start}} + \Delta z_{\text{conv}}} D \, dz}{M_{\text{end}} + \int_{z_{\text{start}}}^{z_{\text{start}} + \Delta z_{\text{conv}}} D \, dz}$$

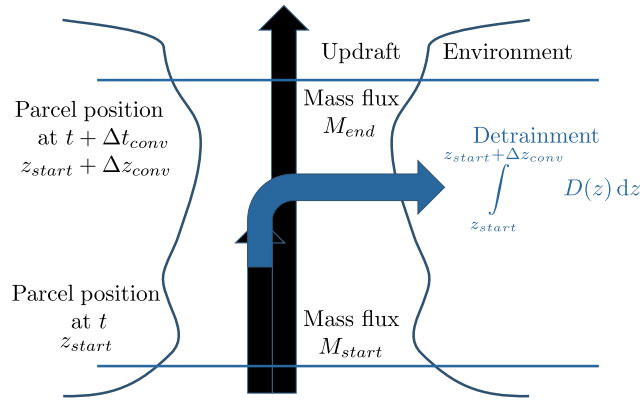


**Figure 2.** Schematic representation of the detrainment step. All quantities are per unit area.

where  $M_{start}$  is the convective mass flux at the start position of the air parcel and  $z_{start}$  is the altitude of the start position.  $z_{start} + \Delta z_{conv}$  is the end position of the air parcel after one intermediate time step (see Figure 2). Conversions from the coordinate system of the trajectory model to geometric altitude are necessary here. The equation is derived  $\Delta t_{conv}$  can be  
 235 determined by noting that ~~all the~~ air involved in convection in the layer defined by  $\Delta z_{conv}$  (regardless whether it ~~was had been~~ entrained in that layer or ~~coming whether it had been transported~~ from below) can only leave via two paths: either it can be detrained or it can leave through the upper boundary. Thus, the detrainment probability is the ratio of the amount of air that is detrained between the start and end position of the air parcel and the sum of the amount of air entering either from below ( $M_{start}$ ) or through entrainment between the start and end position. ~~The equation assumes~~ Assuming that air coming from  
 240 below behaves the same way as ~~air entrained~~. That is, entrained air and that there is no preferred pathway out of the layer for air coming from below or for ~~air entrained~~ entrained air, the detrainment probability is given by

$$\delta = \frac{\int_{z_{start}}^{z_{start} + \Delta z_{conv}} D dz}{M_{start} + \int_{z_{start}}^{z_{start} + \Delta z_{conv}} E dz} \quad (7)$$

or, equivalently

$$\delta = \frac{\int_{z_{start}}^{z_{start} + \Delta z_{conv}} D dz}{M_{end} + \int_{z_{start}}^{z_{start} + \Delta z_{conv}} D dz} \quad (8)$$

245 where  $M_{start}$  is the convective mass flux at the start position of the air parcel and  $z_{start}$  is the altitude of the start position.  $z_{start} + \Delta z_{conv}$  is the end position of the air parcel after one intermediate convective time step (see Figure 2). Conversions from the coordinate system of the trajectory model to geometric altitude are necessary here.

~~Next, another~~ Whether the air parcel is detrained and leaves convection is decided by generating a uniformly distributed random number  $r_r$  ~~is generated~~  $r_{detr}$  and comparing that to the calculated probability  $\delta$ . If the random number is smaller than

250 the detrainment probability  $r_d < \delta r_{\text{detr}} < \delta$ , the parcel leaves the convection at altitude

$$z_{\text{detraindetr}} = z_{\text{start}} + \Delta z_{\text{conv}} \frac{r_d}{\delta} \frac{r_{\text{detr}}}{\delta} \quad (9)$$

Multiplication with  $r_d/\delta r_{\text{detr}}/\delta$  ensures that the detrainment heights are uniformly distributed in  $[z_{\text{start}}, z_{\text{start}} + \Delta z_{\text{conv}}]$ . ~~This is more realistic than assuming  $[z_{\text{start}}, z_{\text{start}} + \Delta z_{\text{conv}}]$ .~~ Assuming that the air parcel always leaves at  $z_{\text{start}} + \Delta z_{\text{conv}}$ . ~~This  $z_{\text{start}} + \Delta z_{\text{conv}}$  would overestimate the detrainment altitude systematically, since  $\delta$  is the probability that the parcel detrains somewhere between  $z_{\text{start}}$  and  $z_{\text{start}} + \Delta z_{\text{conv}}$ .~~ A parcel ~~can~~ is allowed to entrain and detrain in the same ~~trajectory advection~~ time step  $\Delta t$  (but can stay longer in convection, of course).

The approach for detrainment described above differs from the approach employed in previous Lagrangian convective transport schemes, since it takes into account the explicit simulation of the time that air parcels spend in convective updrafts, whereas schemes such as those employed in Collins et al. (2002) or Forster et al. (2007) assume a constant time that parcels spend in convection. The probability that an entrained air parcel detrains at a given altitude, however, is the same in both approaches.

If the parcel reaches an altitude where the convective mass flux  $M$  interpolated to the position of the parcel is zero, but still has not detrained, the parcel is forced to detrain. Due to the finite time step, the air parcel may end up at a position where  $M = 0$ , which can be ~~interpreted~~ interpreted as numerical overshooting. While this behaviour can be avoided by decreasing the altitude of the parcel until  $M > 0$ , we ~~choose not to do not~~ correct for this, since the correction is typically less than 100 m.

If the air parcel detrains before reaching the end of the present ~~trajectory time step advection time step  $\Delta t$  of the trajectory model~~, it cannot entrain again until the start of the next advection time step. A correction can be applied to account for the ~~missing simulated time time missing for new entrainment~~ between the detrainment event (which is at some intermediate ~~time step convective time step  $\Delta t_{\text{conv}}$~~ ) and the start of the next trajectory advection time step. This can be accomplished by adding the missing time to the  $\Delta t$  of the next entrainment test of the trajectory. The effect of this correction is usually small, ~~if the trajectory provided the advection~~ time step is ~~not chosen to large~~ sufficiently small.

The size of the advection time step  $\Delta t$  is crucial. Since the trajectory model ~~output is only on the regular grid of the trajectory time steps~~ generates outputs only every  $\Delta t$  time units, the trajectory is marked as ~~detraining only at the time of the next trajectory detrained only after the next advection~~ time step and not after at the intermediate time step. If the ~~trajectory advection~~ time step is too large, ~~this can have an effect on both the distribution of the residence times in convection (see Figure 12) and on the chemistry of short-lived species (see discussion of SO<sub>2</sub>-like tracer in Section 5)~~ chemical reactions may be overestimated inside of convective clouds.

## 2.6 Subsidence outside of convective systems

To conserve mass and balance the updraft, parcels in the environmental air have to subside. All parcels that are currently not in convection are moved downwards by a pressure difference of

$$\Delta p_{\text{subsidence subs}} = \frac{1}{1 - f_u} \frac{1}{1 - f_{\text{up}}} g_0 M \Delta t \quad (10)$$

where  $M$  and  $f_u f_{\text{up}}$  are the convective mass flux and convective area fraction, respectively, interpolated to the position of the trajectory air parcel. The factor  $1/(1-f_u)$  ~~is a weight introduced to compensate for not subsiding the~~  $1/(1-f_{\text{up}})$  ~~accounts for trajectory air parcels that which are in convection ,but rather than subsiding. Note that this factor is close to unity since  $f_u$  is small~~ since  $f_{\text{up}} \approx 10^{-3}$ . The fraction of ~~trajectories that are in convection will~~ trajectory air parcels which are taking part in convection does not necessarily correlate ~~to  $f_u$  with~~  $f_{\text{up}}$ , which is based on observations independent from the convective parameterization driving the model. However, the results of the validation runs show that the conservation of the vertical mass distribution of the runs is not noticeably affected by this uncertainty (see Section 4).

Alternatively, the fraction of trajectory air parcels that are currently in convection in the model run could be used. This is however only possible for global runs. The mass flux of trajectories through a given surface is not necessarily balanced for non-global ensembles of trajectories. The approach would require to average the results over a volume that is small enough to allow for variations in the fraction, but large enough to contain a sufficient number of air parcels.

Another alternative would be to subside all air parcels and not only the air parcels, which are currently not in convection (Collins et al., 2002). Subsiding air parcels which are currently in convection is however not only unphysical, but also can result in air parcels that descend while they are in convection, and possibly detrain at a lower altitude than they were entrained.

## 2.7 Backward trajectories

~~A nice property~~ An attractive feature of the algorithm is that it ~~also works~~ can be readily employed for backward trajectories. Backward trajectories with convection are useful for e.g. ~~useful for~~ determining the source regions ~~and modelling the chemical composition~~ of air measured along a flight path or sonde ascent and modelling their chemical composition.

~~Some~~ The following modifications of the algorithm are necessary. First, ~~we have to exchange~~ the meaning of  $E$  and  $D$  in the equations has to be exchanged (detrainment becomes entrainment backwards in time). ~~Then, the updraft velocity  $w_u$  has~~ Moreover, the “updraft” velocity  $w_{\text{up}}$  has to be applied with a negative sign. Finally, the correction for subsidence moves the air parcels upward. The “entrainment” probabilities from Equation 3 ~~(actually are now~~ “detrainment probabilities backwards in time”) ~~become,~~ and are given by

$$\varepsilon = \frac{g_0 \Delta t \int_{z(p_k)}^{z(p_{k+1})} D dz}{\Delta p_k} \quad \text{with} \quad \Delta p_k = p_k - p_{k+1} \quad (11)$$

~~The~~ Analogously, the “detrainment” probabilities become “entrainment probabilities backwards in time” with

$$\delta = \frac{\int_{z_{\text{start}} - \Delta z_{\text{conv}}}^{z_{\text{start}}} E dz}{M_{\text{start}} + \int_{z_{\text{start}} - \Delta z_{\text{conv}}}^{z_{\text{start}}} D dz} \quad (12)$$

In contrast to forward trajectories, the convective mass flux at the start position of the air parcel  $M_{\text{start}}$  is at a higher altitude  $z_{\text{start}}$  than the end position  $z_{\text{start}} - \Delta z_{\text{conv}}$ .

If the parcel reaches either an altitude where  $M = 0$  or goes-propagates below the surface (due to the finite time step), but still has not “detrained” the parcel is forced to “detrain”.

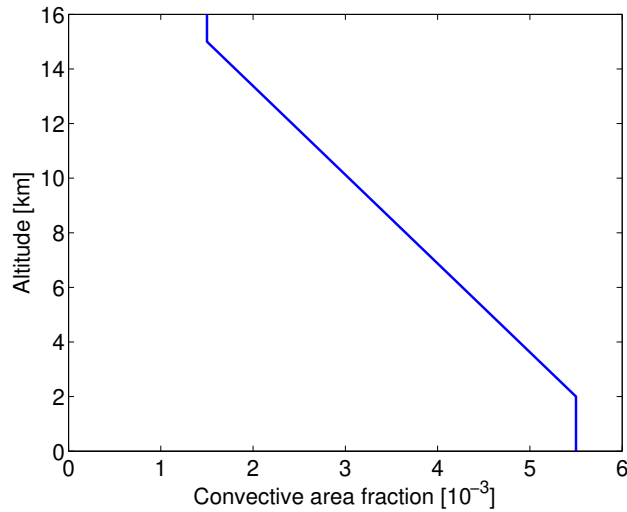


**Figure 3.** Constant convective area fraction profile used for calculating vertical updraft velocities.

### 3 **Simulation of Determining vertical updraft velocities**

Vertical updraft velocities can be calculated by using Equation 4, where most, Except for the convective area fraction  $f_{up}$ , all quantities can be obtained from the meteorological analysis data. However, the convective area fraction  $f_u$  is not available from the meteorological analysis and has to be obtained independently. We implement two methods to estimate  $f_{up}$ , which are described in Sections 3.1 and 3.2.

#### 3.1 Constant convective area fraction

The first method is to use uses a constant climatological profile  $f_u(z)$   $f_{up}(z)$  of the convective area fraction, which is derived from observations. The variability of the vertical velocities is dominated by the variability of the convective mass flux  $M$  for a constant convective area fraction profile (see Equation 4). For this profile, we use C-band dual polarization (CPOL) radar measurements conducted in Darwin, Australia, and define a profile which closely follows

The constant convective area profile used in the method is shown in Figure 3. The profile resembles the profile in Figure 2 of Kumar et al. (2015) (red lines using the “space approach”). The profile, estimating the fraction of convection by comparing the area of convective precipitation to the total measured area). This profile was obtained using C-band dual polarization (CPOL) precipitation radar measurements conducted in Darwin, Australia during two wet seasons (2005/2006 and 2006/2007), and is representative for a  $190 \times 190 \text{ km}^2$  grid box centered over Darwin and is shown in Figure 3. As a result, the variability of the vertical velocities arises mainly from the variability of  $M$  then. The choice of a tropical profile is affected by our first application cases. An obvious shortcoming of this method is that it assumes a globally constant

330 The scanning area of the radar is comparable to typical grid sizes of meteorological analysis data. Kumar et al. (2015) show that the measured mean convective area fraction is independent of the observed area for a wide range of values (from a circle of radius 10 km to a circle of radius 100 km).

Our scheme was originally developed for an application in the tropics. Note that an application of the algorithm in the extratropics would require a different convective area fraction ~~-, which is certainly not realistic~~ profile. We present simulations for the tropics as well as global long-time simulations of radon-222 in Sections 4 and 5. The global simulations however, are not sensitive to the choice of the convective area fraction profile due to the globally constant lifetime of radon (see Section 4.4.4). Hence, ~~we~~ using a tropical profile in the radon runs does not noticeably change the results compared to a run using a profile for the mid-latitudes.

To account for variable convective area fraction profiles as observed in measurements, we now implement a second method ~~to improve on this.~~

### 340 3.2 Random convective area fraction

The second method uses a stochastic parameterization of the convective area fraction ~~conditioned on the large-scale vertical velocity at 500, which is described~~ to obtain randomly drawn convective area fraction profiles and was introduced by Gottwald et al. (2016). The method is based on estimates of convective area fractions derived from CPOL radar measurements over Darwin (wet seasons 2004/2005, 2005/2006, 2006/2007, Davies et al., 2013) and Kwajalein, Marshall Islands (May 2008 to January 2009), averaged over 6 hours. The ~~parameterization depends on the~~ large-scale ~~meteorological state, e.g. the 500hPa vertical velocity, vertical velocity at 500 hPa as an input parameter. The large-scale vertical velocity at 500 hPa~~ was derived by Davies et al. (2013) ~~using a variational analysis~~ by variational analysis using ECMWF operational analysis data constrained by area-mean surface precipitation from the CPOL instrument. Frequency distributions of the convective area fraction are derived from the CPOL measurements as a function of the ~~large-scale large-scale~~ vertical velocity at 500 hPa, ~~see Figs. 1 a and b of Gottwald et al. (2016).~~ Figures 1a and 1b of Gottwald et al. (2016) show the resulting frequency distribution for Darwin and Kwajalein, respectively.

Here, ~~we~~ We combine the Darwin and Kwajalein data into one data set to increase the number of measurements. Peters et al. (2013) and Gottwald et al. (2016) have shown that the functional dependency of convection on the large-scale ~~meteorological state vertical velocity at 500 hPa~~ is sufficiently similar ~~between at~~ both locations.

355 ~~For deriving-~~

To derive the frequency distribution ~~-, used in this study, the combined~~ data are binned into a 2-dimensional lookup table, which uses bins for the ~~large-scale large-scale~~ vertical velocity and bins for the natural logarithm of convective area fraction. The logarithm is used to obtain a more ~~even-uniform~~ distribution over the bins. The ~~resulting lookup table is shown in Figure 4.~~ The data are binned in  $0.005 \text{ m s}^{-1}$  ( $1.2$ ) ~~bins from  $-0.035 \text{ hPa h}^{-1}$~~  bins ranging from  $-0.035 \text{ m s}^{-1}$  to  $0.04$  ~~for the large scale~~  $\text{m s}^{-1}$  for the large-scale vertical velocity and in  $0.5$  bins ~~from  $-12$  to  $-2$  for the~~ ranging from  $-12$  to  $-2$  for the natural logarithm of the convective area fraction. For values of the large-scale vertical velocity greater than  $0.04 \text{ m s}^{-1}$  (smaller than  ~~$-10.2$   $-10.2 \text{ hPa h}^{-1}$~~ ), we use ~~a deterministic relationship~~ the deterministic relationship  $f_{\text{up}} = 0.8807v$  obtained by linear

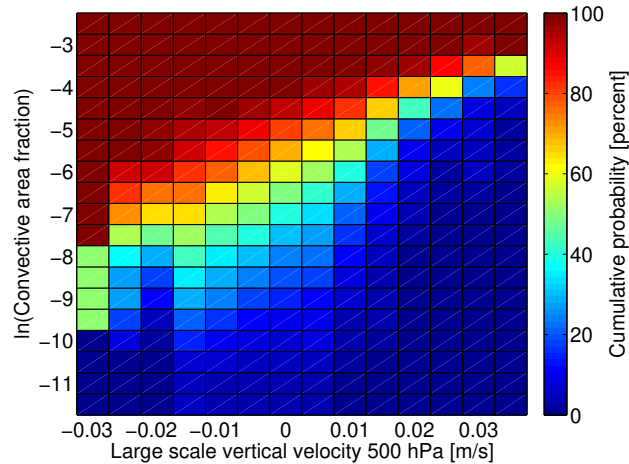


**Figure 4.** Cumulative frequency distribution of the natural logarithm of the convective area fraction from a combined Darwin/Kwajalein CPOL radar dataset as a function of the large-scale vertical velocity at 500 hPa. The distribution is used to calculate the vertical updraft velocities in the algorithm.

regression ~~, since there is not sufficient data for these values of the~~ ( $v$  large-scale vertical velocity in  $\text{m s}^{-1}$ ), as done in Gottwald et al. (2016).

365 The ~~large-scale~~ large-scale vertical velocity of ERA Interim at 500 hPa interpolated to the position of the trajectory air parcel is used to select one of the vertical velocity bins of the frequency distribution. ~~Next, a~~ A uniformly distributed random number is drawn to determine a value for the convective area fraction from the lookup table.

This value is used as the convective area fraction at cloud base. To obtain a vertical profile, the value is then scaled with a normalized version of the profile from Kumar et al. (2015) ~~from the first method. Then, vertical updraft velocities can be~~  
 370 ~~calculated from Equation 4~~ described in Section 3.1. The scaling with a constant profile ensures that the resulting profile of vertical updraft velocities will be physically reasonable (in contrast to a method where the vertical updraft velocity would be obtained independently at every level). ~~Ideally, we would like to draw~~ The vertical updraft velocities are then determined from the convective area ~~fraction at all levels stochastically conditioned on the vertical velocities at all levels. The limited amount of~~  
~~observational data available, however, does not allow for this more involved parametrization~~ fractions using Equation 4.

375 Due to the ~~random stochastic~~ character of the method, it is unavoidable that unrealistic vertical updraft velocities are produced from time to time. ~~This may also be caused by the fact that the method to obtain  $f_u$  does not take into account the value of~~  
~~the convective mass flux at the trajectory position. Hence, values above~~ To prevent unrealistically large values, vertical velocities  
larger than  $20 \text{ m s}^{-1}$  are reset to  $20$ . ~~Values below~~ Values below  $\text{m s}^{-1}$ . Similarly, values smaller than  $0.1 \text{ m s}^{-1}$  are reset to  $0.1 \text{ m s}^{-1}$  to  
 avoid that the ~~trajectories~~ trajectory air parcels remain in convection for too long. ~~This~~ We checked that this procedure only  
 380 affects at most a few percent of the trajectories.

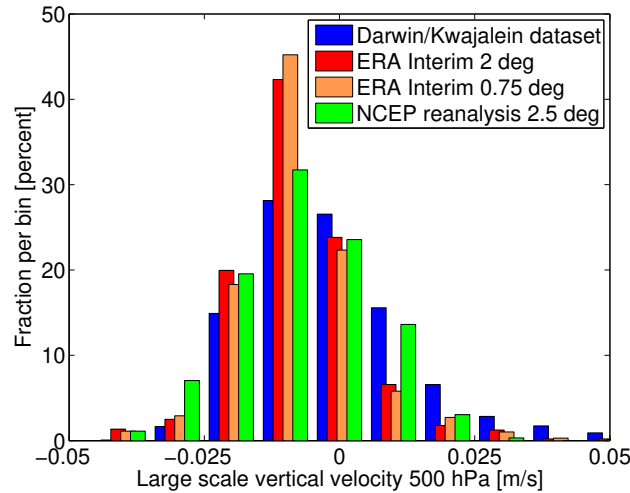


**Figure 5.** Frequency distribution of the vertical velocities at 500 hPa of the Darwin/Kwajalein dataset compared to frequency distributions of the vertical velocity from the ERA Interim reanalysis ( $0.75^\circ \times 0.75^\circ$  and  $2^\circ \times 2^\circ$  horizontal resolution) and the NCEP reanalysis ( $2.5^\circ \times 2.5^\circ$  horizontal resolution). For the reanalysis data, the vertical velocity at 500 hPa at all grid points between  $180^\circ$  E and  $240^\circ$  E and  $30^\circ$  S and  $30^\circ$  N (Pacific Ocean) for the arbitrary date 1 June 2010, 00 h UTC is used. Bin width is  $0.01 \text{ m s}^{-1}$ .

### 3.2.1 Dependency of the stochastic parameterization on the large-scale wind fields and the horizontal resolution

We tacitly assume here that the large-scale vertical velocities of the Darwin/Kwajalein dataset, which are used to determine the convective area fraction profile, and those of the reanalysis are comparable. It is known that differences exist for the large-scale vertical velocities of different reanalysis datasets, which in addition depend on the horizontal resolution of the reanalysis (e.g. Monge-Sanz et al., 2007; Hoffmann et al., 2019). Figure 5 shows the frequency distribution of the vertical velocities at 500 hPa of the Darwin/Kwajalein dataset compared to frequency distributions of the vertical velocity from the ERA Interim reanalysis ( $0.75^\circ \times 0.75^\circ$  and  $2^\circ \times 2^\circ$  horizontal resolution) and the NCEP reanalysis ( $2.5^\circ \times 2.5^\circ$  horizontal resolution, Kistler et al., 2001). For the reanalysis data, the distribution of the large-scale vertical velocity at 500 hPa at all grid points between  $180^\circ$  E and  $240^\circ$  E and  $30^\circ$  S and  $30^\circ$  N is shown (Pacific Ocean). The frequency distributions of all four datasets (including the different horizontal resolutions) agree sufficiently well and differences are acceptable in view of other uncertainties of our method, e.g. the uncertainties of the convective area fraction. Hence, we did not apply a scaling or other correction to the large-scale vertical velocities from ERA Interim. To apply our method to different reanalysis datasets, their vertical velocities at 500 hPa would need to be compared to those of the Darwin/Kwajalein data set, and potentially have to be shifted or scaled to obtain a realistic distribution of the convective area fractions.

The frequency distribution of the measured convective area fractions depends on the size of the measured area from which the frequency distribution is derived. We use the full domain size of the radar of  $190 \times 190 \text{ km}^2$ , which is comparable to a horizontal resolution of the meteorological analysis of about  $2^\circ \times 2^\circ$ . The domain size should be comparable to the grid size

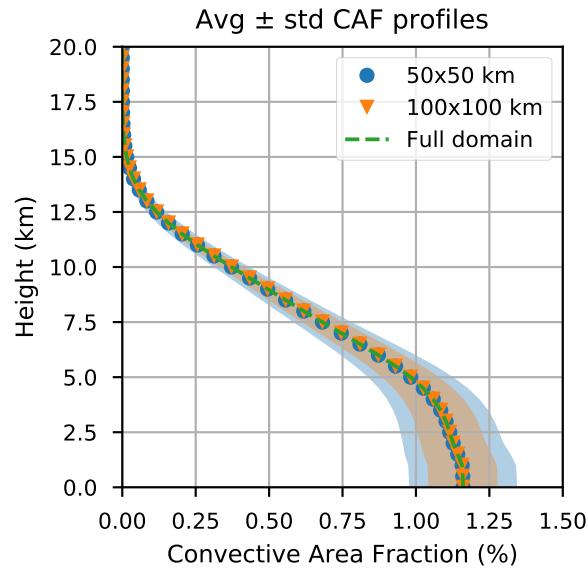


**Figure 6.** Dependence of the standard deviation of the frequency distribution of measured convective area fractions on the used domain size of the CPOL radar. Shaded areas show the standard deviation for a domain size of 190 x 190 km<sup>2</sup> (green), 100 x 100 km<sup>2</sup> (red) and 50 x 50 km<sup>2</sup> (blue). For the smaller domain sizes, the measurement domain of the radar has been divided into smaller subdomains. The shaded areas give the standard deviation. The green line shows the mean convective area fraction.

of the meteorological analysis data to obtain a meaningful distribution of vertical updraft velocities. Smaller domain sizes may produce significant differences in the distribution. As the domain size decreases, the frequency distribution tends to approximate a bimodal distribution: grid cells completely covered by convection and grid cells completely free of convection become more frequent (e.g. Arakawa and Wu, 2013).

Figure 6 shows the dependence of the standard deviation of the frequency distribution of measured convective area fractions on the used domain size of the CPOL radar. Results are shown for domain sizes of 190 x 190 km<sup>2</sup>, 100 x 100 km<sup>2</sup> and 50 x 50 km<sup>2</sup>. For the smaller domain sizes, the measurement domain of the radar is divided into smaller subdomains. The shaded areas give the standard deviation. It is evident that the frequency distributions for different domain sizes differ significantly. The current implementation of the algorithm does not consider this effect, and it is not clear if incorporating a distribution of the convective area fractions which depends on the grid size would lead to a significant change of the results of the trajectory runs. An implementation of frequency distributions of the convective area fractions that depend on grid size is planned for a future version.

### 3.3 Limitations and possible alternatives

~~An alternative approach is to use a climatological profile of measured mean vertical velocities together with some method to obtain variability by scaling the profile, i. e. not to use~~ A limitation of our stochastic parameterization to derive  $f_{up}$  is that we do not take into account the convective mass flux at the position of the trajectory air parcel. Ideally, we would like to use the convective mass flux as the large-scale variable for the stochastic parameterization of the convective area fractions and as a replacement for the large-scale vertical velocity at 500 hPa. This, however, requires observations of convective mass fluxes, which can only be obtained from simultaneous measurements of convective area fractions and updraft velocities (see Kumar et al., 2015).

Alternatively to our approach to estimate the vertical updraft velocity via the convective area fraction and using Equation 4, one might use a climatological profile of measured mean vertical updraft velocities. However, this has the disadvantage that the shape of the wind profile is always the same. To obtain variability in the vertical updraft velocities, a random scaling could be applied to the wind profile. Measurements of updraft velocities are available from in situ aircraft observations (e.g. LeMone and Zipser, 1980), airborne Doppler radar (e.g. Heymsfield et al., 2010) or ground-based wind profilers (e.g. May and Rajopadhyaya, 1999; Kumar et al., 2015). ~~In combination with the given~~ We tested this method with a mean vertical velocity profile taken from Schumacher et al. (2015), but found that the convective area fractions implied from the vertical velocity profile and the convective mass fluxes ~~-, this method of obtaining the vertical updraft velocities may lead to inferred convective area fractions greater than 1-~~ of the meteorological analysis (cf. Equation 4) were greater than 1 in some altitudes. This issue is equivalent to the issue of the unrealistic vertical updraft velocities in the ~~method~~ methods described above using the convective area fractions.

~~A limitation of our method to derive  $f_u$  is that it does not take into account the convective mass flux at the trajectory position. It may be possible to base the~~ A correction for the unrealistic convective area fractions in the approach using a climatological profile of vertical updraft velocities turned out to be more difficult than a correction for the unrealistic vertical updraft velocities in the approach using observations of convective area fractions ~~on convective mass flux as the large scale variable. This requires measured-~~

#### 4 Performance of the convective transport scheme

We examine the performance of our Lagrangian convective transport model by testing the conservation of the vertical mass distribution and the reproduction of the convective mass fluxes ~~-, which can only be obtained from simultaneous measurements of convective area fractions and updraft velocities (see Kumar et al., 2015)~~ and detrainment rates of the meteorological analysis in an idealized trajectory simulation, which ignores the large-scale wind fields. Within the same idealized setup, we show that our method yields vertical updraft velocities which are consistent with observations of velocities larger than  $0.6 \text{ m s}^{-1}$ . We further show results on the residence time of trajectory air parcels in convection. Long-time global trajectory simulations of radon-222, which use the large-scale wind fields, are compared to measurements and global simulations of an artificially designed short-lived  $\text{SO}_2$ -like tracer are used to explore how allowing for variable residence times affects the model results.

## 5 Validation of the convective transport scheme

For validation of the convective transport scheme, we perform trajectory ~~simulations~~ runs driven  
445 by meteorological data of the ECMWF ERA Interim reanalysis (Dee et al., 2011) with  $0.75^\circ \times 0.75^\circ$  or  $2^\circ \times 2^\circ$  horizontal  
resolution, which include ~~large-scale~~ large-scale wind fields, temperature, updraft convective mass fluxes, detrainment rates  
and boundary layer heights. ~~Large-scale~~ Large-scale winds and temperatures are used with 6 h temporal resolution, while  
convective mass fluxes, detrainment rates and boundary layer heights are used with 3 h resolution to capture the diurnal cycle.  
Entrainment rates are not provided by ECMWF and are calculated from the detrainment rates and convective mass fluxes using  
450 Equation 1. The convective parameterization of the ERA Interim reanalysis in the underlying IFS model is originally based on  
the scheme of Tiedtke (1989), with several modifications (e.g. Bechtold et al., 2004). The trajectory ~~model is the model module~~  
is the same that is used in the ATLAS ~~Chemistry and Transport Model~~ chemistry and transport model (Wohltmann and Rex,  
2009), extended for the convective transport scheme. A 4th order Runge-Kutta scheme is used for calculating the trajectories.  
For this study, only the trajectory module of the ATLAS model is used, the detailed chemistry scheme and mixing scheme of  
455 the model are not needed in the model runs (see Section 4.4.1).

While the quality of the ~~used~~ convective mass fluxes and detrainment rates will have a large impact on the results of the ~~Radon~~  
radon validation and the validation of the vertical updraft velocities, it is out of the scope of this study to give a validation of  
ERA Interim. We refer the reader to the existing literature here (e.g. Dee et al., 2011; Taszarek et al., 2018).

### 4.1 ~~Mass conservation~~ Conservation of vertical mass distribution and reproduction of convective mass fluxes and 460 detrainment rates

For ~~the an initial~~ technical verification of the algorithm, we test ~~mass conservation and the reproduction of the archived the~~  
conservation of the vertical mass distribution and examine if our scheme appropriately reproduces the convective mass fluxes  
and detrainment rates. ~~We use a simplified and non-realistic setup here that facilitates interpretation. How well the results of~~  
~~our model compare with reality is an independent issue that will be discussed in Section 4.4 and is examined with a more~~  
465 ~~realistic setup. We also use the more realistic setup to test mass conservation more rigorously later of the reanalysis. We use an~~  
idealized setup here to facilitate the interpretation.

In the ~~simplified~~ idealized setup, we start 100,000 trajectories that are initially uniformly distributed in pressure between  
1000 hPa and 100 hPa and are uniformly distributed horizontally between  $180^\circ$ -E and  $240^\circ$ -E and  $30^\circ$ -S and  $30^\circ$ -N (Pacific  
Ocean). ~~The horizontal domain is chosen due to the flat orography and since the first applications of our model will be in the~~  
470 ~~tropics~~ We impose a horizontal domain without topography to simplify interpretation. The Pacific Ocean is chosen since we are  
mainly interested in applying our model for tropical convection. Each trajectory is assigned a constant mass corresponding to  
the volume it occupies. The runs are driven by temporally constant convective mass fluxes and detrainment rates from ERA  
Interim ( $0.75^\circ \times 0.75^\circ$  horizontal resolution) taken from the ~~arbitrary~~ arbitrarily chosen date 1 June 2010, 00 h UTC. Large-  
scale horizontal and vertical winds are set to zero. ~~I.e., trajectories~~ That is, trajectory air parcels can only move vertically by  
475 convection ~~and subsidence~~. Trajectories that travel inside the cloud or subsidence outside of the cloud. Trajectory air parcels

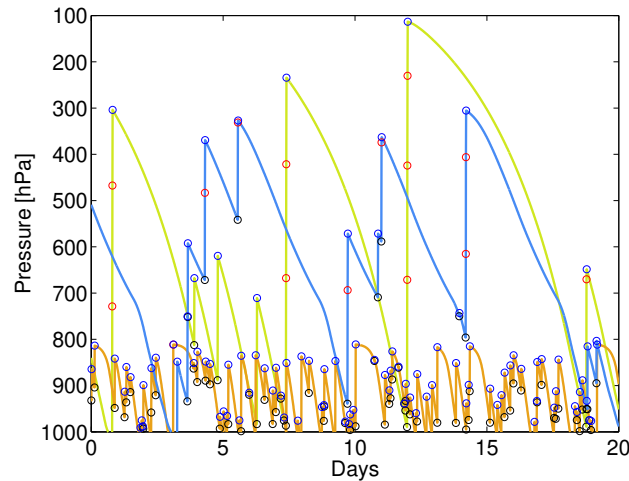
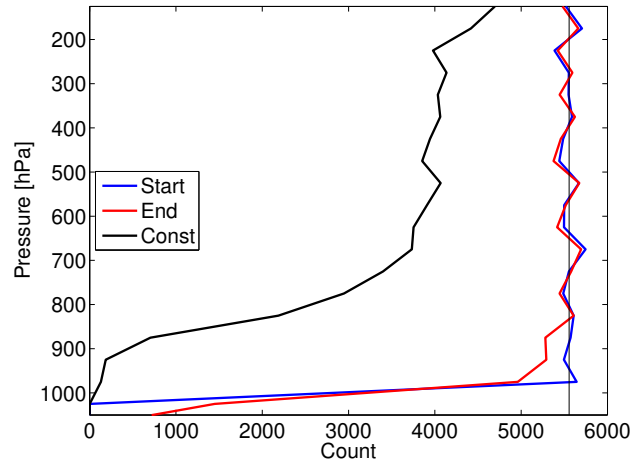


**Figure 7.** Example trajectories from the run with the simplified-idealized setup for forward trajectories with large-scale-large-scale wind set to zero for forward trajectories and constant convective area profile. Open black circles mark entrainment, open red circles upward transport in convection in 10 minute steps and open blue circles detrainment.

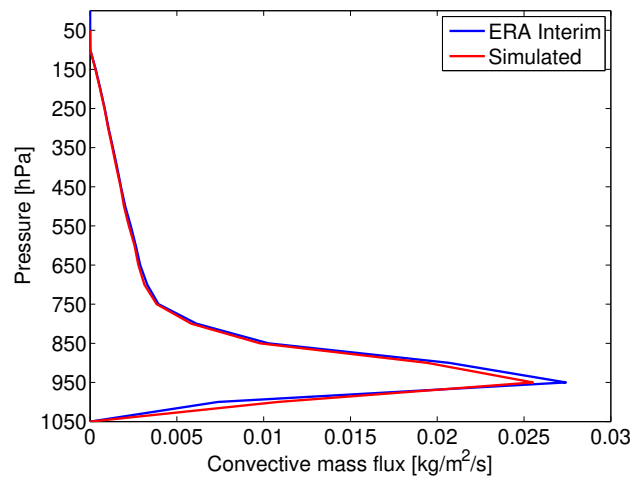
which propagate below the surface due to the finite time step are lifted above the surface again. The trajectory model uses a log-pressure coordinate. Trajectories are run for 20 days, the trajectory time step is with an advection time step  $\Delta t$  of 10 minutes and the trajectory model uses a log-pressure coordinate. Four different runs are performed for forward and backward trajectories and for combined with the two vertical updraft velocity parameterizations (see described in Sections 3.1 and 480 3.2). Each trajectory is assigned a constant mass given by the volume it occupies. Figure 7 shows some arbitrarily selected trajectories from the forward run with when the constant convective area fraction profile (Section 3.1) as examples is used.

Figure 8 shows the mass conservation conservation of the vertical mass distribution for forward trajectories and when the constant convective area fraction profile described in Section 3.1 is used. The number of the trajectories in 50 hPa bins at the start end of the run (blue red) compares well to the number of trajectories in these bins at the end start of the run (red blue). There 485 is only a small deviation at the lowest levels caused by the fact that all trajectories are initialized with pressures lower smaller than 1000 hPa, but that some surface pressures from ERA Interim in the simulated region are higher whereas ERA Interim also features larger values of the surface pressure. This causes some trajectories to end with pressures above at pressures larger than 1000 hPa. Results for backward trajectories or and results employing the random convective or area fraction profile described in Section 3.2 look very similar (not shown).

490 In the simplified-idealized setup, a significant fraction of the trajectories will trajectory air parcels does not move at all, because they are initialized in at a position where the convective mass flux and entrainment rate are zero. In Figure 8, the The number of these trajectories is shown in black in Figure 8. A more rigorous test of mass conservation with a long-term conservation of the vertical mass distribution with a long-time simulation driven by the actual large-scale-large-scale wind fields is shown in the next section presented in Section 4.4.3.



**Figure 8.** ~~Mass conservation~~ Conservation of vertical mass distribution after 20 days for forward trajectories and using a constant convective area fraction profile. Number of trajectories in 50 hPa bins at the start of the run (blue) and at the end of the run (red). The black line denotes the number of trajectories that did not move due to zero convective mass flux at their start position.



**Figure 9.** Mean convective mass flux profile from ERA Interim compared to the simulated convective mass flux profile for forward trajectories and using a constant convective area fraction profile (in a region from 180°-E to 240°-E and 30°-S to 30°-N, 20 days with meteorological fields of 1 June 2010, 00h UTC).

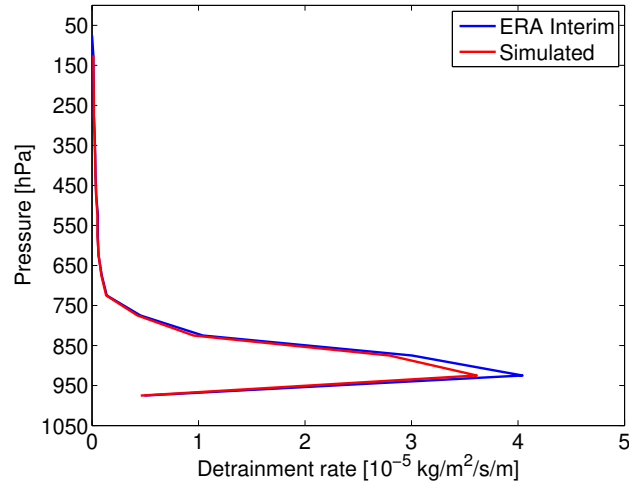


**Figure 10.** Mean detrainment rate profile from ERA Interim compared to the simulated detrainment rate profile for forward trajectories and constant convective area fraction profile (in a region from 180°-E to 240°-E and 30°-S to 30°-N, 20 days with meteorological fields of 1 June 2010, 00h UTC).

495 Figure 9 shows the mean convective mass flux profile from ERA Interim averaged over the tropical domain described above compared with the simulated mass flux profile for forward trajectories ~~and with using~~ the constant convective area fraction profile. Simulated mass fluxes are calculated by counting the ~~trajectories~~ trajectory air parcels that pass a given pressure level during one trajectory advection time step and which are in convection at this time. The number of the trajectories is multiplied ~~with the trajectory mass then by the air parcel mass~~ and divided by the area of the tropical domain and the time period of  
500 20 days. The agreement between ERA Interim and the simulations is very good. There is only a slight underestimation of the pronounced maximum around 950 hPa. ~~Results Again, results~~ for backward trajectories ~~or and results employing the~~ random convective area fraction ~~profiles~~ profile described in Section 3.2 look very similar(~~not shown~~).

Figure 10 shows the same for the detrainment rates. Detrainment rates are calculated by counting the ~~trajectories that have a detrainment event~~ trajectory air parcels which experience detrainment in a given pressure layer during one trajectory advection  
505 time step. The number of ~~the trajectories is multiplied with the trajectory~~ these detained trajectory air parcels is multiplied by the air parcel mass, divided by the area of the tropical domain, the time period of 20 days and the mean vertical extent in geometrical altitude of the pressure layer. Again, agreement is very good and results for backward trajectories or for random convective area fraction profiles look very similar(~~not shown~~).

#### 4.2 ~~Validation of the convection scheme with Radon-222~~

510 While the mean convective mass flux and the detrainment rate profiles are insensitive to the choice of the convective area fraction profile, we see in the following section that the vertical updraft velocity profiles strongly depend on whether a constant convective area profile or a randomly drawn profile is implemented.

## 4.2 Validation of the vertical updraft velocities with wind profiler measurements

515 We validate the modelled vertical updraft velocities against wind profiler measurements. The modelled vertical updraft velocities are taken from the idealized forward trajectory runs in the tropical Pacific from Section 4.1. Results for backward trajectories are very similar.

520 The modelled velocities are compared with measurements from a 50- and 920-MHz wind profiler pair situated in Darwin, Australia. The time resolution of the measurements is 1 minute and vertical updraft velocities are obtained by the method of Williams (2012). Data comprise the wet seasons 2003/2004, 2005/2006, 2006/2007 and 2009/2010. Cloud top heights are determined from the 0 dBz echo top height of the CPOL radar instrument at Darwin. The field of view of this instrument covers the wind profiler site. Convective profiles are identified by using only wind profiler measurements, where the CPOL instrument shows convective precipitation. CPOL data are available every 10 minutes. All wind profiler measurements within  $\pm 5$  minutes of the CPOL measurement times are considered and cut at the corresponding cloud top height.

525 Figure 11 shows frequency distributions of the vertical updraft velocities binned in  $0.2 \text{ m s}^{-1}$  bins for selected 50 hPa pressure bins. The frequency distributions of the vertical updraft velocities from the Darwin measurements are shown in black, modelled distributions employing the constant convective area fraction profile are shown in magenta and modelled distributions employing random convective area fraction profiles are shown in red. The solid lines show the distributions when vertical updraft velocities smaller than  $0.6 \text{ m s}^{-1}$  are excluded, while the dashed lines show distributions comprised of all velocity values.

530 There is a large number of measurements with small vertical updraft velocities. The sensitivity of the measured distributions to these small values is quite large, and the measured distributions excluding values smaller than  $0.6 \text{ m s}^{-1}$  differ significantly from the measured distributions which incorporate all values. The distributions obtained from our scheme show considerably less values smaller than  $0.6 \text{ m s}^{-1}$  and there is less of a difference between the modelled distributions when all velocities or only those larger than  $0.6 \text{ m s}^{-1}$  are accounted for.

535 It is difficult to assess the reasons for the marked disagreement between model and measurements in the small vertical updraft velocities. The number of small values is sensitive to the method to determine convective situations in the wind profiler measurements, and may change significantly depending on the method. It is common to apply a lower threshold to the vertical updraft velocities to define convective situations (e.g. LeMone and Zipser, 1980; May and Rajopadhyaya, 1999; Kumar et al., 2015). Typically, this threshold is between  
540  $0 \text{ m s}^{-1}$  and  $1.5 \text{ m s}^{-1}$  and may have a significant effect (see discussion in Kumar et al., 2015). Hence, part of the disagreement can be attributed to the conceptual problem of defining what a convective updraft is.

545 For the modelled profiles, the distribution of the velocities is determined by a large number of factors and may change significantly depending on the details of implementation and the convective parameterization in the underlying meteorological analysis. For example, the assumed convective area fraction profile and the assumptions in the Tiedtke scheme plays a large role. Hence, we do not expect more than a qualitative agreement between model and measurements, in particular for small

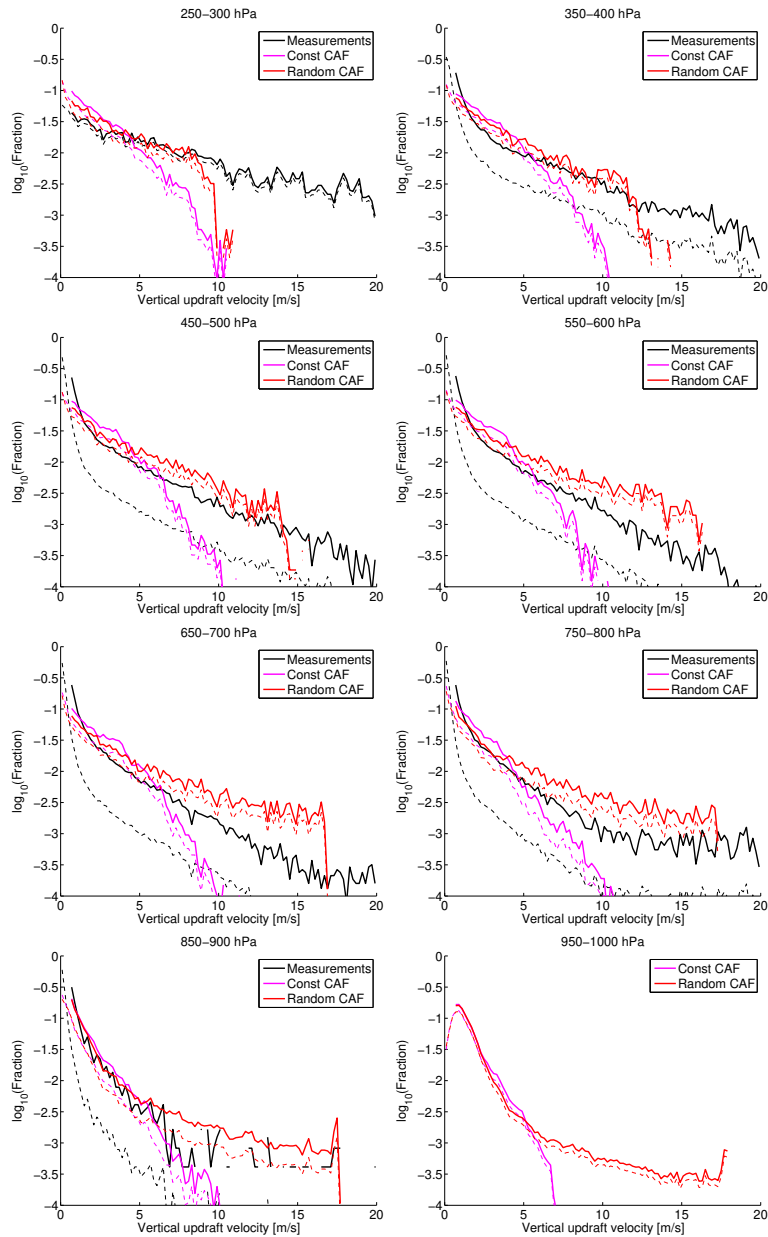


**Figure 11.** Frequency distribution of vertical updraft velocities for different pressure bins from wind profiler measurements in Darwin, Australia, in  $0.2 \text{ m s}^{-1}$  bins (black), compared to the corresponding frequency distributions of vertical updraft velocities obtained from the constant and random convective area fraction profile method (magenta and red). The dashed lines show the distribution including all velocity values ( $> 0 \text{ m s}^{-1}$ ), for the solid lines all values below  $0.6 \text{ m s}^{-1}$  are excluded.

updraft velocities. The lower threshold of  $0.1 \text{ m s}^{-1}$  implemented into our convective transport scheme (see Section 3.2) should however play no role in Fig. 11, since the bin width is  $0.2 \text{ m s}^{-1}$ .

550 The distribution of the vertical updraft velocities reproduces the distribution of the measurements fairly well, when only velocities greater than  $0.6 \text{ m s}^{-1}$  are considered. In particular, the magnitude of the approximately exponential decrease in the frequency distribution is met well.

In the case when random convective area fraction profiles are employed our method yields a higher frequency of large vertical velocities compared to the case when the constant convective area fraction profile is implemented. The random convective area fraction profile method leads to a better agreement with observations. In particular, the two implementations differ significantly for values of the vertical updraft velocity larger than  $5 \text{ m s}^{-1}$ .

555 The fact that the vertical updraft velocities are typically larger when a randomly drawn convective area fraction profile is used can be readily understood qualitatively: Assuming that  $M$ ,  $T$  and  $p$  are fixed, the mean updraft velocity in case of a mean constant convective area fraction profile  $\langle f_{\text{up}} \rangle$  is simply  $\langle w_{\text{up}1} \rangle = \frac{MRT}{\langle f_{\text{up}} \rangle p}$ , where  $\langle \dots \rangle$  denotes the mean over all air parcels. In the case of a varying randomly drawn convective area fraction profile, the mean vertical updraft velocities need to be expressed as  $\langle w_{\text{up}2} \rangle = \langle \frac{MRT}{f_{\text{up}} p} \rangle = \frac{MRT}{p} \langle \frac{1}{f_{\text{up}}} \rangle$ . Since  $\langle \frac{1}{f_{\text{up}}} \rangle \geq \frac{1}{\langle f_{\text{up}} \rangle}$  due to the fact that the harmonic mean is always smaller  
560 than the geometric mean, we obtain the relation  $\langle w_{\text{up}2} \rangle \geq \langle w_{\text{up}1} \rangle$  between the mean vertical updraft velocities of the two implementations. This implies that also individual realizations of  $w_{\text{up}}$  are on average larger for the random convective area fraction profiles.

565 Replacing the simulated vertical updraft velocities by the measured vertical updraft velocities in the model (including values smaller than  $0.6 \text{ m s}^{-1}$ ) would increase the average residence time between entrainment and detrainment. In turn, this would lead to a lower concentration of a short-lived species like  $\text{SO}_2$  in the upper troposphere.

The model is trained on convective area fraction data measured in Darwin and Kwajalein and compared to wind profiler data measured at Darwin, while it is applied to a larger region covering a large part of the tropical Pacific here. The lack of other measurements does not allow for a completely independent model validation.

### 4.3 Residence time in convection

570 Figure 12 shows the frequency distribution of the residence times of the trajectories between entrainment and detrainment obtained from simulations employing both parameterizations for the vertical updraft velocity (solid lines). Most convective events have a residence time of less than 30 minutes (more than 95 % when the constant convective area fraction profile is implemented). Since the number of convective events is dominated by shallow convective events, which typically only lift the air parcel a few hundred meters in one advection time step (cf. Figure 7), we also show the frequency distribution for deep  
575 convection (dashed lines), defined here by detrainment events above 300 hPa. These will be more relevant when considering the upper tropospheric mixing ratio of short-lived species. Typical residence times of deep convective events are estimated to be about 1 hour when the constant convective area fraction profile is implemented. The simulation using random convective area fraction profiles yields a higher number of convective events with a short residence time and correspondingly, a lower number of convective events with long residence times, compared to the simulation using the constant convective area fraction

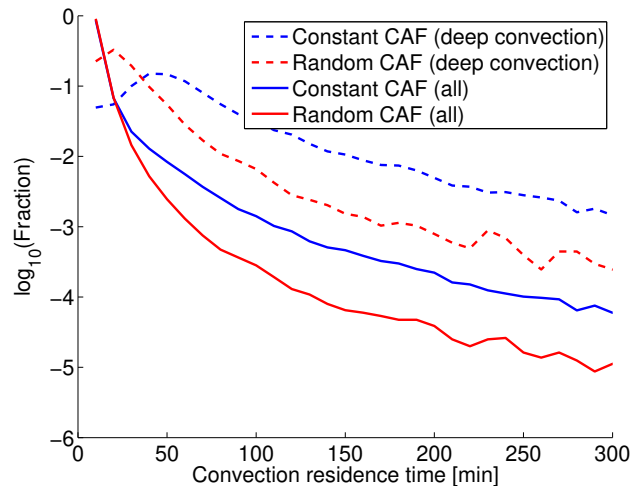


**Figure 12.** Frequency distribution of the residence times of the trajectories between entrainment and detrainment simulated by the two parameterizations for the vertical updraft velocity. The fraction of all events with a given duration is shown in 10 minute bins. Solid lines show the distribution for all convective events, while dashed lines show the contribution from deep convective events (detrainment above 300 hPa).

580 profile. This is consistent with the larger simulated vertical updraft velocities when using randomly generated convective area fraction profiles.

#### 4.4 Comparison of long-time simulations of radon-222 with aircraft measurements

A validation with measurement data is performed by comparing the results of long-term Long-time global trajectory simulations of Radon-222 to measurements. These results will depend radon-222 are compared here with aircraft observations. The results depend to a great extent on the used meteorological data. They are presented here to demonstrate that the model is able to produce reasonable results with a given meteorological analysis.

Radon-222 is formed by the radioactive decay of uranium in rock and soils and has been widely used to validate convection models and to evaluate tracer transport (e.g. Jacob et al., 1997; Feng et al., 2011). Its popularity is due to some favorable properties: (e.g. Feichter and Crutzen, 1990; Mahowald et al., 1995; Jacob et al., 1997; Collins et al., 2002; Forster et al., 2007; Feng et al., 2011) . It is chemically inert, is not subject to wet and dry deposition and is only removed by radioactive decay. Hence, its removal processes are very well known. The half-life time of 3.8 days is in the right order of magnitude to detect changes in convective transport. However, the measurement coverage of Radon radon is quite limited (in particular for profiles) and emissions ,which can vary with region and time, are uncertain (e.g. Liu et al., 1984; Mahowald et al., 1995). Furthermore, the globally constant lifetime of radon does not allow for any validation of the parameterization of the vertical updraft velocities. Nevertheless, radon-222 is currently widely used for validation of convective transport due to a lack of alternatives.

#### 4.4.1 Setup of the radon runs

Global runs are performed for the time period 1 January 1989 to 31 December 2005. Trajectories are initialized at random positions ~~with 150~~(both horizontally and in pressure) between 1100~~horizontal resolution in layers of hPa and 50 hPa from~~  
600 ~~1100~~. The number of trajectories is chosen in such a way that the mean horizontal distance of the trajectories is 150 to km  
in reference to a layer of a width of 50 hPa. The random positioning is the default initialization in ATLAS and avoids that  
an initialization on a regular grid can have any systematic effects on the results. Trajectories initialized below ~~surface are~~  
~~deleted~~the surface are discarded. The trajectory model uses a log-pressure coordinate and is driven by ERA Interim data. ~~The~~  
~~trajectory time step~~with a horizontal resolution of  $2^\circ \times 2^\circ$ . The advection time step  $\Delta t$  is set to 30 minutes. Trajectories that  
605 ~~travel~~The change from 10 minutes to 30 minutes and from  $0.75^\circ \times 0.75^\circ$  to  $2^\circ \times 2^\circ$  is due to computational constraints. We  
performed 1-year test runs with a  $0.75^\circ \times 0.75^\circ$  resolution, a 10 minute time step and a mean horizontal distance of 75 km of  
the trajectories that show that the results of the run with the lower horizontal and time resolution are nearly identical.

Trajectory air parcels which propagate below the surface due to the finite time step are lifted above the surface~~again~~. In the  
uppermost layer (100 hPa to 50 hPa), ~~trajectory positions are reinitialized at random positions in~~the positions of the trajectory  
610 air parcels are reinitialized to random positions at every time step. There is no special treatment of the boundary layer except  
for the assumption of a well-mixed layer when distributing the ~~Radon emissions. There is also no radon emissions. We do not~~  
~~apply any~~ mixing of air parcels to simulate diffusion, contrary to the stratospheric version of the model (Wohltmann and Rex,  
2009). Given the resolution of the model runs and the short half-life time of ~~Radon~~radon, we believe that these simplifications  
are justified.

615 ~~Figure 13 shows the mass conservation of the long-term simulation. The number of trajectories in 50 bins at the start of a~~  
~~run with convection and the constant~~ Note that the convective area fraction profile (cyan) compares very well with the mass  
distribution at the end of the run (magenta) and the results of a run without convection (blue and red). The lower number  
of trajectories in the bins near the surface is due to orography. The trajectories remain homogeneously distributed in the  
horizontal domain without clustering or forming gaps over the course of the model run, and hence no further measures are  
620 ~~applied to redistribute trajectories (not shown used (see Fig. 3) is only appropriate for the tropics. However, the radon runs~~  
~~are not sensitive to the convective area fraction profile due to the globally constant lifetime of radon (see the discussion in~~  
Section 4.4.4).

#### 4.4.2 Radon emissions

We use the same ~~Radon emissions as in~~radon emissions as e.g. Jacob et al. (1997) and Feng et al. (2011). Radon is  
625 emitted almost exclusively over land. The radon emissions are  $1.0 \text{ atoms cm}^{-2} \text{ s}^{-1}$  over land between  $60^\circ \text{S}$ – $60^\circ \text{N}$ ,  
 $0.005 \text{ atoms cm}^{-2} \text{ s}^{-1}$  over oceans between  $60^\circ \text{S}$ – $60^\circ \text{N}$ ,  $0.005 \text{ atoms cm}^{-2} \text{ s}^{-1}$  between  $60^\circ$  and  $70^\circ$  in both hemi-  
spheres~~and zero polewards of~~. There is no emission between  $70^\circ$  and the poles. These emissions are considered to be accurate  
on a global scale to within 25 % and on a regional scale to about a factor of 2 (Jacob et al., 1997; Forster et al., 2007). Radon is  
emitted into all trajectory air parcels that are in the boundary layer. ~~Boundary layer height is taken from ERA Interim. Radon~~

630 ~~is distributed evenly over these parcels~~ by assuming a well-mixed boundary layer, ~~which means adding and~~ a volume mixing ratio ~~of  $x$  of~~

$$\tilde{x} = \frac{e \Delta t}{\Delta z_{\text{BL}}} \frac{k_B T}{p} \quad (13)$$

~~is added~~ to each air parcel in the boundary layer, where  $e$  is the emission in atoms per area and time interval,  $\Delta t$  is the ~~trajectory model time step~~,  $k_B = 1.38 \cdot 10^{-23} \text{ J/K}$  ~~advection time step of the trajectory model~~,  $k_B = 1.38 \cdot 10^{-23} \text{ JK}^{-1}$  is the Boltzmann constant and  $\Delta z_{\text{BL}}$  is the local height of the boundary layer. ~~The boundary layer height is provided by ERA Interim.~~

To avoid large horizontal areas ~~without any trajectories that receive Radon in which no trajectory air parcels receive radon~~ emissions, a minimum boundary layer height of 500 m is used. ~~While the~~ ~~The~~ factor  $1/\Delta z_{\text{BL}}$  would still ensure mass conservation if no minimum boundary layer height is assumed (~~the decreasing number of air parcels that receive emissions in a given area receiving emissions when decreasing the height of the boundary layer is balanced by the increasing concentration in the~~ fewer parcels that receive emissions), ~~emissions~~. ~~However, the uptake of emissions by trajectories would become patchy and the horizontal resolution of the emission fields would not be fully used. This is especially relevant for species with strongly spatially varying emissions like  $\text{SO}_2$ .~~

Our approach may cause some radon which would be trapped in the boundary layer to be emitted immediately into the free troposphere and may cause some differences of the simulation to the radon measurements. However, assuming a minimum boundary layer height (or some similar measure) is unavoidable, since the required number of trajectories needed for a model run which resolves the boundary layer by far exceeds currently available computational capabilities.

#### 4.4.3 Conservation of vertical mass distribution

We revisit the issue of the conservation of the vertical mass distribution in this more realistic setup, compared to the idealized setup in Section 4.1. Figure 13 shows the conservation of the vertical mass distribution of air (not of radon) of the long-time simulation. The number of trajectory air parcels in 50 hPa bins at the end of a run with convection and the constant convective area fraction profile (magenta) compares very well with the number of trajectory air parcels at the start of the run (cyan) and the results of a run without convection (red and blue). The lower number of trajectory air parcels in the bins near the surface is due to orography. The trajectory air parcels remain homogeneously distributed in the horizontal domain without clustering or forming gaps over the course of the model run, confirming that no further measures are required to redistribute trajectories.

#### 655 4.4.4 Comparison with measurements

~~Unfortunately, there is only a limited number of vertical profile measurements of Radon.~~ We compare the simulations to the climatological mid-latitude profiles of Liu et al. (1984), which have been widely used to validate tracer transport in global models in the past (~~e.g. Collins et al., 2002; Feng et al., 2011~~) (~~e.g. Feichter and Crutzen, 1990; Jacob et al., 1997; Collins et al., 2002; Feng et al., 2011~~). These observations were obtained from aircraft measurements at different continental locations in the northern midlatitudes from 1952 to 1972. Figure 14 shows the ~~mean simulated Radon~~ ~~simulated mean radon~~ profile for June to August over land ( $30^\circ\text{-N}$ – $60^\circ\text{-N}$ ) compared to the

Liu et al. (1984) mean measurement profile for the same season (from 23 sites, bars show standard deviation of the profiles). ~~Simulations~~ Simulation results are averaged over all 15 years of the ~~long-term~~ long-time run, but the years are not identical to the years of measurement, since there is no meteorological data from ERA Interim for this time period. Figure 15 shows the same for December to February (7 sites, no standard deviation available).

~~In addition~~ Furthermore, we show ~~comparisons~~ a comparison of our simulated radon activity to aircraft campaign measurements from coastal locations around Moffett Field (37.5°-N, 122°-E, California) in June and August 1994 (Kritz et al., 1998) in Figure 16 (Kritz et al., 1998) ~~and to~~ and a comparison with aircraft measurements from coastal regions in Eastern Canada (Nova Scotia) from the North Atlantic Regional Experiment (NARE) campaign in August 1993 (Zaucker et al., 1996) in Figure 17 (Zaucker et al., 1996). Simulation results are averaged over the campaign periods and over a longitude-latitude bounding box encompassing all aircraft measurements.

The ~~agreement~~ runs with convection generally show higher radon concentrations than the runs without convection in the middle and upper troposphere due to the fast transport of radon from the boundary layer to the detrainment level. A more detailed interpretation of the profiles is however difficult due to the large-scale horizontal averaging.

The agreement of the simulations to the measurements is reasonable, given the large uncertainties in measurements and emissions. ~~Runs~~ While the runs with convection agree better with the measurements than the runs without convection, ~~there are still significant differences. For the same radon measurements, differences of a similar order of magnitude are also observed in other studies and for other convective transport models (e.g. Collins et al., 2002; Forster et al., 2007; Feng et al., 2011).~~

There is an underestimation of ~~Radon~~ radon by the simulations in the middle troposphere, which is most pronounced in the Moffett Field data (Figure 16), consistent with previous studies (e.g. Jacob et al., 1997; Forster et al., 2007). This may be ~~caused by~~ due to uncertainties in emission and due to the fact that ~~several measurements are~~ measurements from coastal areas ~~, where the Radon gradient is~~ are included, where horizontal radon gradients are high and difficult to model (see also Forster et al., 2007).

The results for both vertical updraft velocity parameterizations are nearly identical because of the globally constant lifetime of ~~Radon~~ (a radon. A globally constant lifetime implies that for an air parcel in a given layer, only the time since the last contact with the boundary layer matters and not the exact path that the trajectory air parcel has taken to the layer). ~~For the same reason, an almost instantaneous redistribution of air parcels as in Collins et al. (2002) will also lead to results very similar to the results shown for the two vertical updraft velocity parameterizations. Hence, it is not possible to give a recommendation for one of the vertical updraft velocity parameterizations from the results of the Radon simulations.~~

~~For this reason, we perform runs with a SO<sub>2</sub>-like tracer with a varying lifetime in Section 5. Unfortunately, species like SO<sub>2</sub>, where different vertical updraft velocity parameterizations lead to significantly different tracer concentrations are often difficult to validate with measurements. This is due to the large uncertainties in the chemistry schemes and microphysics for these species, uncertain emissions and sparse measurement coverage.~~

~~Long term mass conservation after 15 years for a run with forward trajectories and the constant convective area fraction profile, compared to a run without convection. Number of trajectories in 50 bins at the start of the run (blue and cyan) and at the end of the run (red and magenta).~~

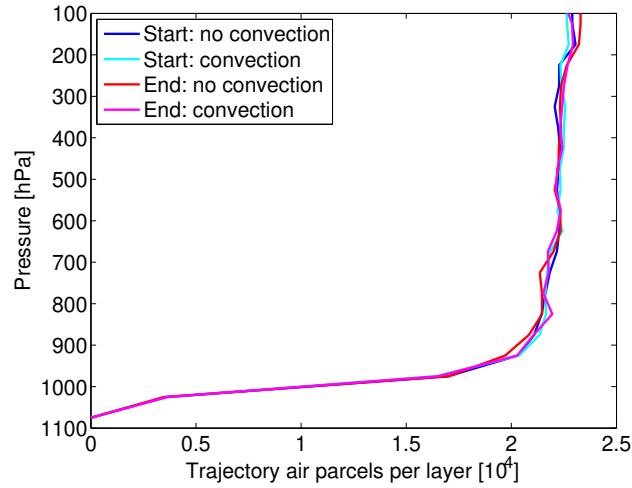


**Figure 13.** Long-time conservation of the vertical mass distribution after 15 years for a run with forward trajectories using the constant convective area fraction profile and for a run without convection. We show the number of trajectory air parcels in 50 hPa bins at the start of the run (blue and cyan) and at the end of the run (red and magenta).

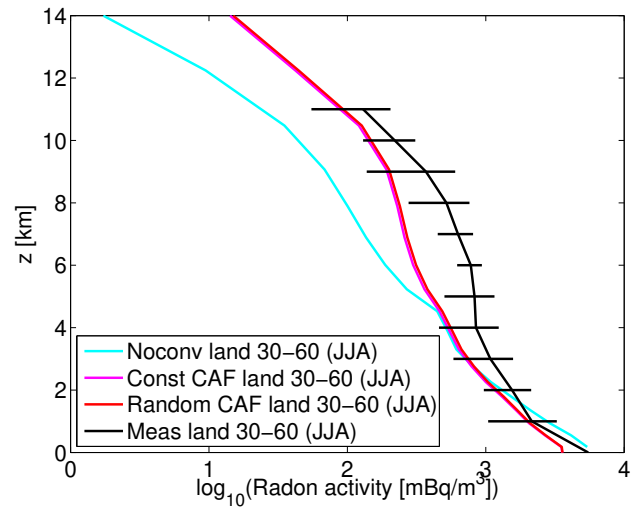


**Figure 14.** Observed mean radon profile obtained from measurements over land ( $30^{\circ}$  N– $60^{\circ}$  N, June–August) by Liu et al. (1984) compared to the simulated radon obtained from 15 year long-time runs for the same region and months. Bars show the standard deviation of the profiles.

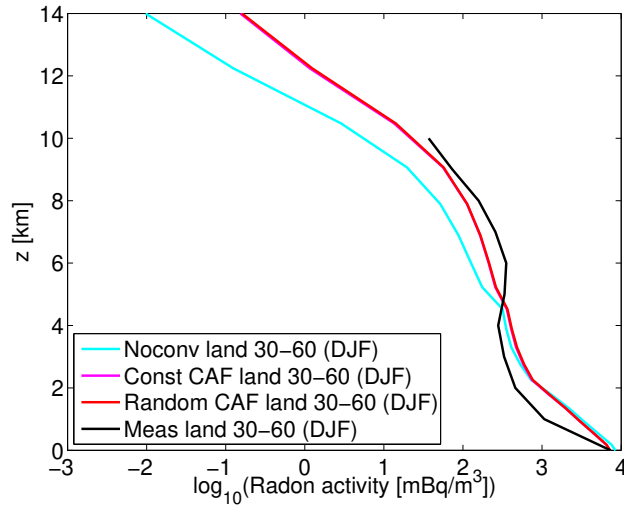


**Figure 15.** Observed mean radon profile obtained from measurements over land (30° N–60° N, December–February) by Liu et al. (1984) compared to the simulated radon obtained from 15 year long-time runs for the same region and months.

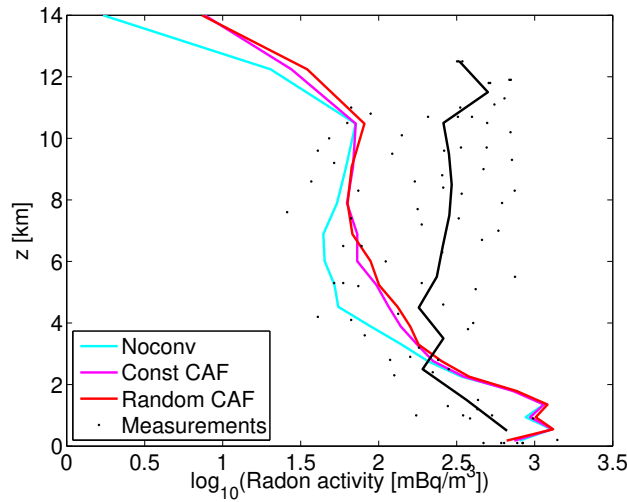


**Figure 16.** Observed radon from aircraft measurements of the Moffett Field campaign (California) in June 1994 (Kritz et al., 1998) compared to the simulated radon from our model in the same time period using a bounding box including all measurements. Dots show the single measurements and the solid black line the mean in 1 km bins.

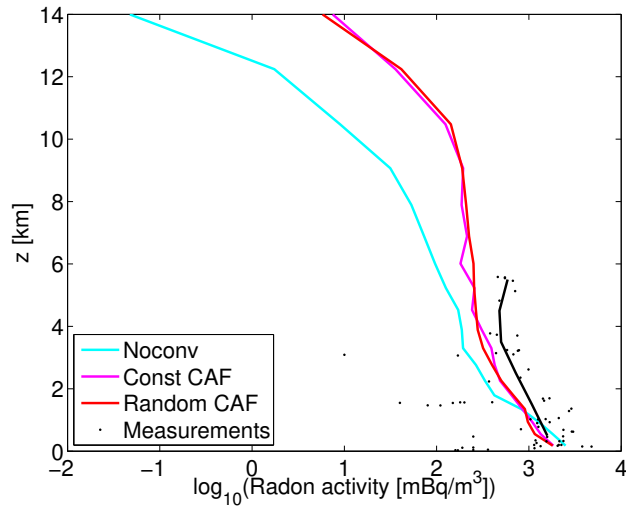


**Figure 17.** Observed radon from aircraft measurements of the North Atlantic Regional Experiment (NARE) campaign in August 1993 (Zaucker et al., 1996) compared to the simulated radon from our model in the same time period using a bounding box including all measurements. Dots show the single measurements and the solid black line the mean in 1 km bins.

Mean observed radon profile measured over land (30 N–60 N, June–August) from Liu et al. (1984) compared to the simulated Radon from a 15 year long term run for the same region and months. Bars show the standard deviation of the profiles:

700 Mean observed radon profile measured over land (30 N–60 N, December–February) from Liu et al. (1984) compared to the simulated Radon from a 15 year long term run for the same region and months.

Observed radon from aircraft measurements of the Moffett Field campaign (California) in June 1994 (Kritz et al., 1998) compared to the simulated Radon in the same time period and a bounding box including all measurements. Dots show the single measurements and the solid black line the mean in 1 bins.

705 Observed radon from aircraft measurements of the North Atlantic Regional Experiment (NARE) campaign in August 1993 (Zaucker et al., 1996) compared to the simulated Radon in the same time period and a bounding box including all measurements. Dots show the single measurements and the solid black line the mean in 1 bins.

#### 4.5 Validation of the vertical updraft velocities with wind profiler measurements

710 Modelled vertical updraft velocities are validated by comparison to wind profiler measurements. The modelled vertical updraft velocities are taken from the simplified forward trajectory run in the tropical Pacific from Section 4.1. Results for backward trajectories are very similar (not shown).

The modelled velocities are compared statistically with measurements from a 50- and 920-wind profiler pair situated in Darwin, Australia. The time resolution of the measurements is 1 and vertical updraft velocities are obtained by the method

of Williams (2012). Data comprise the wet seasons 2003/2004, 2005/2006, 2006/2007 and 2009/2010. Cloud top heights are  
715 determined from the 0-echo top height of the CPOL radar instrument at Darwin. The field of view of this instrument covers  
the wind profiler site. Convective profiles are identified by using only measurements that show convective precipitation in the  
CPOL measurements. CPOL data are available every  $\approx 10$  min. It makes no difference if a trajectory air parcel was transported slowly  
upwards from the emission in the boundary layer to 10 km. All wind profiler measurements within  $\pm 5$  km of the CPOL measurement  
times are considered and cut at the corresponding cloud top height.

720 Figure 11 shows frequency distributions of the vertical updraft velocities binned in 0.2 m/s bins and for selected 50 pressure  
bins. Frequency distributions of the vertical updraft velocities from the Darwin measurements are shown in black, modelled  
distributions from the constant convective area fraction profile method are shown in magenta and modelled distributions from  
random convective area fraction profile method are shown in red. The solid lines show the distributions with all measurements  
and all modelled values below 0.6 km excluded, while the dashed lines show distributions with all velocity values included.

725 Frequency distribution of vertical updraft velocities for different pressure bins from wind profiler measurements in Darwin,  
Australia, in 0.2 m/s bins (black), compared to the corresponding frequency distributions of vertical updraft velocities obtained  
from the constant and random convective area fraction profile method (magenta and red). The dashed lines show the distribution  
including all velocity values ( $> 0$ ), for the solid lines all values below 0.6 km are excluded.

730 There is a high number of measurements with small vertical updraft velocities. The sensitivity of the measured distribution  
to the many small values is quite large, and the measured distributions cut at 0.6 km differ significantly from the measured  
distributions showing all values. The modelled distributions show considerably less values below 0.6 km, and the modelled  
distributions cut at 0.6 km agree well with the modelled distributions showing all values.

735 The agreement between the measurements and the modelled values for the random convective area fraction method is quite  
satisfactory, when only velocities greater than 0.6 km are considered, giving some confidence in the method. In particular, the magnitude of the exponential decrease in the  
frequency distribution is met quite well. Using the random convective area fraction profile method clearly leads to higher  
vertical velocities on average than using the constant convective area fraction profile. I.e., the random convective area fraction  
profile method shows a higher frequency of large vertical velocities than the constant convective area fraction profile method,  
which is in better agreement with observations. The agreement of the measurements to the modelled values from the constant  
740 convective area fraction method is worse for values of more than 5 km than for the random convective area fraction method.

745 It is difficult to say what the reason for the marked disagreement between model and measurements in the  
small vertical updraft velocities is. The number of small values is sensitive to the method to determine convective  
situations in the wind profiler measurements, and may change significantly depending on the method. It is common  
in other publications to apply a lower threshold to the vertical updraft velocities to obtain convective profiles  
(e.g. LeMone and Zipser, 1980; May and Rajopadhyaya, 1999; Kumar et al., 2015). For the modelled profiles, the distribution  
of the velocities is determined by a large number of factors and may change significantly depending on the details of  
implementation and the convective parameterization in the underlying meteorological analysis. E.g., the assumed convective

area fraction profile and the assumptions in the Tiedtke scheme will play a large role for 9 days and 23 hours. For the same reason, a convective redistribution of air parcels with a fixed time step as in Collins et al. (2002) leads to similar results. Hence, we don't expect more than a qualitative agreement between model and measurements.

Note that the model is trained on convective area fraction data measured in Darwin and Kwajalein and compared to wind profiler data measured at Darwin, while it is applied to a larger region covering a large part of the tropical Pacific here. The lack of other measurements does not allow for a completely independent model validation.

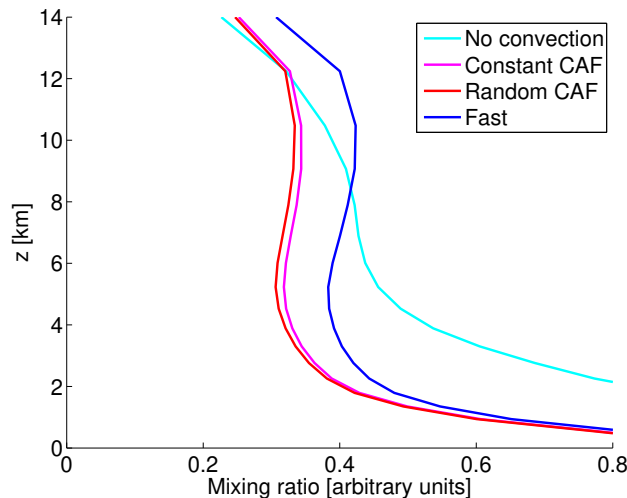
#### 755 4.5 Residence time in convection

Figure 12 shows the frequency distribution of the residence times of the trajectories between entrainment and detrainment simulated by the two parameterizations for the vertical updraft velocity (solid lines). It is evident that most convective events have a residence time of less than 30 minutes (more than 95% for the constant convective area fraction profile). Since the number of convective events is dominated by shallow convective events, which typically only lift the air parcel a few 100 in one trajectory time step (see Figure 7), we also show the frequency distribution for deep convection (approximated by detrainment events above 300). These will be more relevant for the upper tropospheric mixing ratio of short-lived species. Typical residence times of deep convective events are around 1 hour for the constant convective area fraction profile. The simulation with the random convective area fraction profile shows a higher number of convective events with a short residence time and correspondingly, a lower number with long residence time, compared to the simulation with constant convective area fraction profile. This is consistent with the larger simulated vertical updraft velocities for the random profile parameterizations from the results of the radon simulations.

Frequency distribution of the residence times of the trajectories between entrainment and detrainment simulated by the two parameterizations for the vertical updraft velocity. Shown is the fraction of all events with a given duration in 10 minute bins. Solid lines show the distribution for all convective events, while dashed lines show the contribution from deep convective events (detrainment above 300).

### 5 Simulations with a SO<sub>2</sub>-like tracer

To demonstrate that there is a benefit to explicitly simulate the vertical updraft velocity and to account for a variable time spent in convective clouds, we perform by performing runs with an artificial tracer that is designed to imitate the most important characteristics of the short-lived species SO<sub>2</sub>, which unlike radon has a varying lifetime (a detailed model of SO<sub>2</sub> chemistry and emissions is complex and is outside the scope of this study). SO<sub>2</sub> transported from the troposphere to the stratosphere is one of the most important contributors to the stratospheric aerosol layer in volcanically quiescent periods (see e.g. the review in Kremser et al., 2016). In addition, SO<sub>2</sub> is a pollutant mainly produced by anthropogenic sources, which is responsible for atmospheric acidification and for the direct and indirect aerosol effect (e.g. Feichter et al., 1996; Berglen et al., 2004; Tsai et al., 2010).



**Figure 18.** Mean simulated artificial  $\text{SO}_2$ -like tracer profiles in the tropics ( $30^\circ\text{-S}$ – $30^\circ\text{-N}$ ) for a run without convection, a run with a constant convective area fraction profile, a run with a random convective area fraction profile and a run where the vertical updraft velocity is set to a constant value of  $100\text{ m s}^{-1}$  to mimic the ~~almost instantaneous~~-redistribution within a short fixed time step in other Lagrangian convective transport schemes.

780  $\text{SO}_2$  is depleted by a gas-phase reaction with OH and by several fast heterogenous reactions in the liquid phase in clouds (~~mainly by~~, mainly with  $\text{H}_2\text{O}_2$ ) (see e.g. Berglen et al., 2004; Tsai et al., 2010; Rollins et al., 2017). The lifetime with respect to the OH reaction is ~~on of~~ the order of days to weeks (e.g. Rex et al., 2014), while the lifetime in the presence of clouds is ~~on of~~ the order of hours to days (e.g. Lelieveld, 1993). Hence, we perform runs with ~~a~~ an artificially designed tracer which has a lifetime of 0.1 days when in convection and of 10 days when not in convection. Emissions are distributed uniformly over the globe. ~~Trajectory time step~~ The advection time step of the trajectory model is 10 minutes. The horizontal resolution of ERA Interim is  $0.75^\circ \times 0.75^\circ$  and only one year is simulated.

Four different runs are performed: a run without convection, a run with a constant convective area fraction profile, a run with random convective area fraction profiles and a run where the vertical updraft velocity is set to a constant value of  $100\text{ m s}^{-1}$  (with  $\Delta t_{\text{conv}}$  set to 1 s) to mimic the ~~almost instantaneous redistribution in other~~-redistribution of trajectory air parcels in a short fixed time step as in previous Lagrangian convective transport schemes (e.g. Collins et al., 2002). ~~The setup of the runs is identical to the Radon runs, except again that only one year is simulated~~ For chemical species with a varying lifetime such as  $\text{SO}_2$ , different vertical updraft velocity parameterizations lead to significantly different tracer concentrations. Such short-lived species are often difficult to validate with measurements. This is due to the large uncertainties in the chemistry schemes and microphysics for these species, uncertain emissions and sparse measurement coverage (see discussion in e.g. Forster et al., 2007).

795 Figure 18 shows the mean simulated  $\text{SO}_2$ -like tracer profiles in the tropics ( $30^\circ\text{-S}$ – $30^\circ\text{-N}$ ) for the four different runs. The run without convection ~~shows larger values~~ leads to larger values of the mixing ratio than the other runs in the lower troposphere,

since ~~without convection~~ the tracer is ~~always~~-depleted with a long lifetime of 10 days. ~~The runs with convection show smaller values due to the fast depletion,~~ whereas with convection fast depletion occurs in the convective cloud. ~~In clouds,~~ leading to a smaller mixing ratio. Conversely, in the upper troposphere, the run without convection ~~shows lower values than the other runs,~~ since the transport times yields lower values of the mixing ratio than the runs involving convection, since without convection it takes much longer for a trajectory air parcel to be transported to the upper troposphere ~~are much longer atmosphere.~~ Residence times in the clouds are shortest in the run ~~without convection.~~ ~~In the runs with convection,~~ larger vertical updraft velocities lead to shorter residence times in the cloud, and hence, to higher values of the tracer where we set the vertical updraft velocity to the large value of  $100 \text{ m s}^{-1}$ , leading to the largest mixing ratios in the upper atmosphere for this method.

While the ~~difference~~ differences in the mixing ratios between the run ~~with the almost instantaneous redistribution involving a redistribution in a short time period~~ and the runs ~~using the employing~~ convective area fraction ~~is~~ profiles are significant, the two schemes ~~for the using~~ convective area fraction profiles for the computation of the vertical updraft velocities only show a small difference. ~~This means that~~ Hence, for the  $\text{SO}_2$ -like tracer, the scheme is robust with respect to the ~~exact~~ particular parameterization of the vertical updraft velocities, as long as the order of magnitude of the velocities is ~~right~~ correct.

~~We will briefly discuss implications of the differences in the simulations of short-lived species in the model runs and stress their scientific relevance in modelling the time spent in convective updrafts. A more quantitative assessment is outside the scope of this study and is planned for future studies.~~

Differences in  $\text{SO}_2$  in the upper troposphere can have an impact on the radiation balance of the Earth and on stratospheric ozone depletion, since they affect the stratospheric aerosol layer (e.g. Rollins et al., 2017). The lower transport of  $\text{SO}_2$  into the stratosphere in our scheme compared to a scheme with a redistribution in a fixed time step implies a lower contribution of  $\text{SO}_2$  to the stratospheric aerosol layer, and hence e.g. a lower impact of changes in  $\text{SO}_2$  emissions in India or China on the stratospheric aerosol layer. A quantitative assessment of this effect, however, is challenging due to large uncertainties in measurements (e.g. Rollins et al., 2017), chemistry and microphysics (e.g. Kremser et al., 2016).

$\text{SO}_2$  is a pollutant mainly produced by anthropogenic sources, which is amongst others responsible for atmospheric acidification and the direct and indirect aerosol effect (e.g. Feichter et al., 1996; Berglen et al., 2004; Tsai et al., 2010). Our results suggest that compared to a scheme with a fixed redistribution time step, more  $\text{SO}_2$  would be converted to  $\text{H}_2\text{SO}_4$  by heterogeneous reactions in cloud droplets in the lower troposphere.

Another example for which changes in the convective transport times could be relevant is the contribution of very short-lived bromine substances (VSLS) to the stratospheric bromine budget, which is relevant for stratospheric ozone depletion (e.g. Hossaini et al., 2012). While the lifetime of most VSLS (e.g.  $\text{CH}_3\text{Br}$ ,  $\text{CH}_2\text{Br}_2$ ) is too long to be of relevance here, changes of the convective transport times may be relevant for inorganic product gases produced by the VSLS, which are susceptible to washout (e.g.  $\text{HBr}$ ,  $\text{HOBr}$ ) (e.g. Schofield et al., 2011; Hossaini et al., 2012; Wales et al., 2018).

## 6 Conclusions

830 We present a newly developed new Lagrangian convective transport scheme for Chemistry and Transport Models and ensemble trajectory simulations chemistry and transport models. The scheme is driven by convective mass fluxes and detrainment rates from meteorological data or General Circulation Models and relies on that originate from an external convective parameterization. Our scheme extends the usual approach used in Lagrangian models of statistically redistributing air parcels within a fixed time step by modelling the time that an air parcels spends inside the convective event . This is important for correctly  
835 simulating the chemistry of short-lived species in the troposphere and may be crucial for determining their mixing ratios in the upper troposphere (e.g. Hoyle et al., 2011). As an example, we show that there is a significant effect on the mixing ratios of SO<sub>2</sub> when using our scheme compared to a scheme with a nearly instantaneous redistribution of air parcels (see Figure 18), which can be obtained from meteorological analysis data or general circulation models. The novelty of our method is that we explicitly model the variable time that a trajectory air parcel spends in a convective event by estimating vertical updraft velocity profiles,  
840 in contrast to the common approach of a vertical redistribution of air parcels in a fixed time period. Vertical updraft velocities are obtained from combining convective mass fluxes from the meteorological analysis data with a parameterization of convective area fraction profiles. Convective area fractions are obtained by two different parameterizations: a parameterization using a constant convective area profile as well as a parameterization which uses randomly drawn profiles to allow for variability.

Runs are performed We performed simulations with the convective transport model implemented into the ATLAS Chemistry and Transport Model (e.g. Wohltmann and Rex, 2009) and are trajectory module of the ATLAS chemistry and transport model (e.g. Wohltmann and Rex, 2009), which were driven by ECMWF ERA Interim reanalysis data (Dee et al., 2011).

The algorithm is successfully validated by showing that the Our scheme is able to reproduce the convective mass fluxes and detrainment rates from the meteorological analysis data within a few percent. Mass conservation Conservation of the vertical mas distribution in a global 15 year trajectory simulation is also within a few percent, with no apparent trend.

850 Two parameterizations for the vertical updraft velocities are tested and compared to wind profiler measurements conducted at Darwin, Australia. The two parameterizations use either a constant or a random convective area fraction profile. Frequency distributions of the modelled vertical velocities agree well with the measurements for the random convective area fraction method and wind profiler measurements conducted at Darwin, Australia, for vertical velocities larger than 0.6 , but show some discrepancies for small vertical velocities or the m s<sup>-1</sup>. The agreement was markedly better for the parameterization using a randomly drawn convective area fraction profile than for a constant convective area fraction method. However, it turns out that it is a favorable property of the scheme that the results for chemical tracers are robust with respect to the exact parameterization of the vertical updraft velocities, as long as the order of magnitude of the velocities is right. profile.

860 Global long-term long-time trajectory simulations of Radon-222 driven by the ECMWF ERA Interim reanalysis and using the convective transport scheme are performed to examine how well the model compares to observations. The runs show a reasonable agreement to the measurements. It is however difficult to draw clear conclusions from the validation with these measurement data due to the large uncertainties in emissions, radon-222 were performed and compared to observations. The agreement to the measurements is reasonable, given the large uncertainties in emissions and measurements

of radon. Uncertainties in emissions, measurements, chemistry and microphysics of short-lived species generally pose a challenge to the validation of simulations of these species, and there is a clear need to improve on this situation (as also noted by e.g. Forster et al., 2007).

An accurate simulation of the ~~limited amount of measurements and the dependence on the used meteorological data used by the convective transport scheme~~ time spent in clouds is important for correctly simulating the chemistry of short-lived species in the troposphere and may be crucial for determining their mixing ratios in the upper troposphere (e.g. Hoyle et al., 2011). As an example for a species for which this is relevant we consider SO<sub>2</sub>, which is depleted by fast heterogenous reactions in clouds and by a gas-phase reaction with OH. SO<sub>2</sub> transported from the troposphere to the stratosphere is one of the most important contributors to the stratospheric aerosol layer in volcanically quiescent periods (e.g. Kremser et al., 2016). In addition, SO<sub>2</sub> is a pollutant mainly produced by anthropogenic sources (e.g. Berglen et al., 2004). Allowing for a variable time that an air parcel spends in convection yields a significant effect on the mixing ratios of an SO<sub>2</sub>-like tracer compared to assuming a redistribution of air parcels in a fixed time step (cf. Figure 18). Remarkably, the mixing ratio distributions were insensitive to the choice of the parameterization of the convective area fraction profile, as long as the order of magnitude of the implied vertical updraft velocities is correct (cf. Figure 18).

Future work ~~will include e.g. and improvements of the method will include~~ the simulation of downdrafts ~~and improvements in clouds as well as extensions for applications~~ in the mid-latitudes. For this work, we largely concentrated on the performance in the tropics, the region of the first application cases.

So far, the scheme has been applied ~~in the calculation of the origin and convective properties of air sampled during flights of the StratoClim campaign, and has been used for~~ calculations of ammonia transport (Höpfner et al., 2019). A future study ~~will simulate the~~ transport and chemistry ~~calculations~~ of SO<sub>2</sub> to ~~determine-examine~~ the contribution of SO<sub>2</sub> to the stratospheric sulfur burden. ~~These application cases will be presented in separate studies~~ aerosol layer.

*Code and data availability.* The source code is available on the AWIForge repository (<https://swrepo1.awi.de/>). Access to the repository is granted on request under the given correspondence address. This work is based on the revision 1279 of the version control system. Radon climatological profile data over land for the NH mid-latitude region was obtained from Liu et al. (1984). The aircraft radon measurements of the Moffett field and NARE data are available from the Table 1 in Kritz et al. (1998) and Table 3 in Zaucker et al. (1996), respectively. Vertical wind profiler data are available upon request to Alain Protat ([alain.protat@bom.gov.au](mailto:alain.protat@bom.gov.au)).

*Author contributions.* IW and RL developed and validated the convection model. MR initiated the model development and contributed to the discussion. GG and KP provided the stochastic model for the convective area fraction and contributed to the discussion. WF contributed to the discussion and provided the radon data. AP provided the Darwin wind profiler data and contributed to the analysis of the vertical velocity comparisons. VL provided the CPOL cloud top heights extracted over the Darwin profiler site. CW produced the dual-frequency vertical air velocity retrievals.

*Competing interests.* The authors declare that they have no conflict of interest.

895 *Acknowledgements.* This research has received funding from the European Community's Seventh Framework Programme (FP7/2007–2013) under grant agreement no. 603557 (StratoClim). We thank ECMWF for providing reanalysis data and Holger Deckelmann for his support in handling and obtaining the ECMWF data. Thanks go to Benjamin Segger for his work on Figures 1 and 2.

## References

- Arakawa, A.: The cumulus parameterization problem: past, present, and future, *J. Clim.*, 17, 2493–2525, 2004.
- 900 Arakawa, A. and Wu, C.-M.: A Unified Representation of Deep Moist Convection in Numerical Modeling of the Atmosphere. Part I, *J. Atmos. Sci.*, 70, 1977–1992, 2013.
- Bechtold, P., Chaboureau, J.-P., Beljaars, A., Betts, A. K., Köhler, M., Miller, M., and Redelsperger, J.-L.: The simulation of the diurnal cycle of convective precipitation over land in a global model, *Quart. J. Roy. Meteorol. Soc.*, 130, 3119–3137, 2004.
- Berglen, T. F., Berntsen, T. K., Isaksen, I. S. A., and Sundet, J. K.: A global model of the coupled sulfur/oxidant chemistry in the troposphere: 905 The sulfur cycle, *J. Geophys. Res.*, 109, D19310, <https://doi.org/10.1029/2003JD003948>, 2004.
- Collins, W. J., Derwent, R. G., Johnson, C. E., and Stevenson, D. S.: A comparison of two schemes for the convective transport of chemical species in a Lagrangian global chemistry model, *Quart. J. Roy. Meteorol. Soc.*, 128, 991–1009, 2002.
- Davies, L., Jakob, C., May, P., Kumar, V. V., and Xie, S.: Relationships between the large-scale atmosphere and the small-scale convective state for Darwin, Australia, *J. Geophys. Res.*, 118, 11 534–11 545, <https://doi.org/10.1002/jgrd.50645>, 2013.
- 910 Dee, D. P., Uppala, S. M., Simmons, A. J., Berrisford, P., Poli, P., Kobayashi, S., Andrae, U., Balmaseda, M. A., Balsamo, G., Bauer, P., Bechtold, P., Beljaars, A. C. M., van de Berg, L., Bidlot, J., Bormann, N., Delsol, C., Dragani, R., Fuentes, M., Geer, A. J., Haimberger, L., Healy, S. B., Hersbach, H., Hólm, E. V., Isaksen, L., Kållberg, P., Köhler, M., Matricardi, M., McNally, A. P., Monge-Sanz, B. M., Morcrette, J.-J., Park, B.-K., Peubey, C., de Rosnay, P., Tavolato, C., Thépaut, J.-N., and Vitart, F.: The ERA-Interim reanalysis: configuration and performance of the data assimilation system, *Q. J. R. Meteorol. Soc.*, 137, 553–597, 2011.
- 915 Feichter, J. and Crutzen, P.: Parameterization of vertical tracer transport due to deep cumulus convection in a global transport model and its evaluation with <sup>222</sup>Radon measurements, *Tellus*, 42B, 100–117, 1990.
- Feichter, J., Kjellström, E., Rodhe, H., Dentener, F., Lelieveld, J., and Roelofs, G.-J.: Simulation of the tropospheric sulfur cycle in a global climate model, *Atmos. Environ.*, 30, 1693–1707, 1996.
- Feng, W., Chipperfield, M. P., Dhomse, S., Monge-Sanz, B. M., Yang, X., Zhang, K., and Ramonet, M.: Evaluation of cloud convection and 920 tracer transport in a three-dimensional chemical transport model, *Atmos. Chem. Phys.*, 11, 5783–5803, 2011.
- Forster, C., Stohl, A., and Seibert, P.: Parameterization of convective transport in a Lagrangian particle dispersion model and its evaluation, *J. Appl. Meteorol. Clim.*, 46, 403–422, 2007.
- Gottwald, G. A., Peters, K., and Davies, L.: A data-driven method for the stochastic parametrisation of subgrid-scale tropical convective area fraction, *Quart. J. Roy. Meteorol. Soc.*, 142, 349–359, 2016.
- 925 Heymsfield, G. M., Tian, L., Heymsfield, A. J., Li, L., and Guimond, S.: Characteristics of deep tropical and subtropical convection from nadir-viewing high-altitude airborne Doppler radar, *J. Atmos. Sci.*, 67, 285–308, 2010.
- Hoffmann, L., Günther, G., Li, D., Stein, O., Wu, X., Griessbach, S., Heng, Y., Konopka, P., Müller, R., Vogel, B., and Wright, J. S.: From ERA-Interim to ERA5: the considerable impact of ECMWF's next-generation reanalysis on Lagrangian transport simulations, *Atmos. Chem. Phys.*, 19, 3097–3124, 2019.
- 930 Höpfner, M., Ungerer, J., Borrmann, S., Wagner, R., Spang, R., Riese, M., Stiller, G., Appel, O., Batenburg, A. M., Bucci, S., Cairo, F., Dragoneas, A., Friedl-Vallon, F., Hünig, A., Johansson, S., Krasaukas, L., Legras, B., Leisner, T., Mahnke, C., Möhler, O., Mollenker, S., Müller, R., Neubert, T., Orphal, J., Preusse, P., Rex, M., Saathoff, H., Strohm, F., Weigel, R., and Wohltmann, I.: Ammonium nitrate particles formed in upper troposphere from ground ammonia sources during Asian monsoons, *Nature Geoscience*, 2019.

- Hossaini, R., Chipperfield, M. P., Feng, W., Breider, T. J., Atlas, E., Montzka, S. A., Miller, B. R., Moore, F., and Elkins, J.: The contribution of natural and anthropogenic very short-lived species to stratospheric bromine, *Atmos. Chem. Phys.*, 12, 371–380, 2012.
- 935 Hoyle, C. R., Marécal, V., Russo, M. R., Allen, G., Arteta, J., Chemel, C., Chipperfield, M. P., D’Amato, F., Dessens, O., Feng, W., Hamilton, J. F., Harris, N. R. P., Hosking, J. S., Lewis, A. C., Morgenstern, O., Peter, T., Pyle, J. A., Reddmann, T., Richards, N. A. D., Telford, P. J., Tian, W., Viciani, S., Volz-Thomas, A., Wild, O., Yang, X., and Zeng, G.: Representation of tropical deep convection in atmospheric models – Part 2: Tracer transport, *Atmos. Chem. Phys.*, 11, 8103–8131, 2011.
- 940 Jacob, D. J., Prather, M. J., Rasch, P. J., Shia, R.-L., Balkanski, Y. J., Beagley, S. R., Bergmann, D. J., Blackshear, W. T., Brown, M., Chiba, M., Chipperfield, M. P., de Grandpré, J., Dignon, J. E., Feichter, J., Genthon, C., Grose, W. L., Kasibhatla, P. S., Köhler, I., Kritz, M. A., Law, K., Penner, J. E., Ramonet, M., Reeves, C. E., Rotman, D. A., Stockwell, D. Z., Velthoven, P. F. J. V., Verver, G., Wild, O., Yang, H., and Zimmermann, P.: Evaluation and intercomparison of global atmospheric transport models using  $^{222}\text{Rn}$  and other short-lived tracers, *J. Geophys. Res.*, 102, 5953–5970, 1997.
- 945 Kistler, R. E., Kalnay, E., Collins, W., Saha, S., White, G., Woollen, J., Chelliah, M., Ebisuzaki, W., Kanamitsu, M., Kousky, V., van den Dool, H., Jenne, R., and Fiorino, M.: The NCEP-NCAR 50-year reanalysis: Monthly means CD-ROM and documentation, *Bull. Amer. Meteorol. Soc.*, 82, 247–268, 2001.
- Kremser, S., Thomason, L. W., von Hobe, M., Hermann, M., Deshler, T., Timmreck, C., Toohey, M., Stenke, A., Schwarz, J. P., Weigel, R., Fueglistaler, S., Prata, F. J., Vernier, J.-P., Schlager, H., Barnes, J. E., Antuña-Marrero, J.-C., Fairlie, D., Palm, M., Mahieu, E., Notholt, J., Rex, M., Bingen, C., Vanhellemont, F., Bourassa, A., Plane, J. M. C., Klocke, D., Carn, S. A., Clarisse, L., Trickl, T., Neely, R., James, A. D., Rieger, L., Wilson, J. C., and Meland, B.: Stratospheric aerosol – Observations, processes, and impact on climate, *Rev. Geophys.*, 54, 278–335, <https://doi.org/10.1002/2015RG000511>, 2016.
- 950 Kritz, M. A., Rosner, S. W., and Stockwell, D. Z.: Validation of an off-line three-dimensional chemical transport model using observed radon profiles: 1. Observations, *J. Geophys. Res.*, 103, 8425–8432, 1998.
- 955 Kumar, V. V., Jakob, C., Protat, A., Williams, C. R., and May, P. T.: Mass-Flux characteristics of tropical cumulus clouds from wind profiler observations at Darwin, Australia, *J. Atmos. Sci.*, 72, 1837–1855, 2015.
- Lelieveld, J.: Multi-Phase Processes in the Atmospheric Sulfur Cycle, in: *Interactions of C, N, P and S Biogeochemical Cycles and Global Change*, edited by Wollast, R., Mackenzie, F. T., and Chou, L., pp. 305–331, Springer, New York, 1993.
- LeMone, M. A. and Zipser, E. J.: Cumulonimbus vertical velocity events in GATE. Part I: Diameter, intensity and mass flux, *J. Atmos. Sci.*, 37, 2444–2457, 1980.
- 960 Liu, S. C., McAfee, J. R., and Cicerone, R. J.: Radon 222 and tropospheric vertical transport, *J. Geophys. Res.*, 89, 7219–7292, 1984.
- Mahowald, N. M., Rasch, P. J., and Prinn, R. G.: Cumulus parameterizations in chemical transport models, *J. Geophys. Res.*, 100, 26 173–26 189, 1995.
- May, P. T. and Rajopadhyaya, D. K.: Vertical velocity characteristics of deep convection over Darwin, Australia, *Mon. Weather Rev.*, 127, 1056–1071, 1999.
- 965 Monge-Sanz, B. M., Chipperfield, M. P., Simmons, A. J., and Uppala, S. M.: Mean age of air and transport in a CTM: Comparison of different ECMWF analyses, *Geophys. Res. Lett.*, 34, L04801, <https://doi.org/10.1029/2006GL028515>, 2007.
- Peters, K., Jakob, C., Davies, L., Khouider, B., and Majda, A. J.: Stochastic Behavior of Tropical Convection in Observations and a Multicloud Model, *J. Atmos. Sci.*, 70, 3556–3575, <https://doi.org/10.1175/JAS-D-13-031.1>, 2013.

- 970 Rex, M., Wohltmann, I., Ridder, T., Lehmann, R., Rosenlof, K., Wennberg, P., Weisenstein, D., Notholt, J., Krüger, K., Mohr, V., and Tegtmeier, S.: A tropical West Pacific OH minimum and implications for stratospheric composition, *Atmos. Chem. Phys.*, 14, 4827–4841, 2014.
- Rollins, A. W., Thornberry, T. D., Watts, L. A., Yu, P., Rosenlof, K. H., Mills, M., Baumann, E., Giorgetta, F. R., Bui, T. V., Höpfner, M., Walker, K. A., Boone, C., Bernath, P. F., Colarco, P. R., Newman, P. A., Fahey, D. W., and Gao, R. S.: The role of sulfur dioxide in stratospheric aerosol formation evaluated by using in situ measurements in the tropical lower stratosphere, *Geophys. Res. Lett.*, <https://doi.org/10.1002/2017GL072754>, 2017.
- 975 Rossi, D., Maurizi, A., and Fantini, M.: IL-GLOBO (1.0) – development and verification of the moist convection module, *Geosci. Model Dev.*, 9, 789–797, 2016.
- Schofield, R., Fueglistaler, S., Wohltmann, I., and Rex, M.: Sensitivity of stratospheric Br<sub>y</sub> to uncertainties in very short lived substance emissions and atmospheric transport, *Atmos. Chem. Phys.*, 11, 1379–1392, 2011.
- 980 Schumacher, C., Stevenson, S. N., and Williams, C. R.: Vertical motions of the tropical convective cloud spectrum over Darwin, Australia, *Quart. J. Roy. Meteorol. Soc.*, 141, 2277–2288, 2015.
- Taszarek, M., Brooks, H. E., Czernecki, B., Szuster, P., and Fortuniak, K.: Climatological Aspects of Convective Parameters over Europe: A Comparison of ERA-Interim and Sounding Data, *J. Clim.*, 31, 4281–4308, 2018.
- 985 Tiedtke, M.: A comprehensive mass flux scheme for cumulus parameterization in large-scale models, *Mon. Wea. Rev.*, 117, 1779–1800, 1989.
- Tsai, L.-C., Chen, J.-P., Lin, P.-Y., Wang, W.-C., and Isaksen, I. S. A.: Sulfur cycle and sulfate radiative forcing simulated from a coupled global climate-chemistry model, *Atmos. Chem. Phys.*, 10, 3693–3709, 2010.
- 990 Wales, P. A., Salawitch, R. J., Nicely, J. M., Anderson, D. C., Canty, T. P., Baidar, S., Dix, B., Koenig, T. K., Volkamer, R., Chen, D., Huey, L. G., Tanner, D. J., Cuevas, C. A., Fernandez, R. P., Kinnison, D. E., Lamarque, J.-F., Saiz-Lopez, A., Atlas, E. L., Hall, S. R., Navarro, M. A., Pan, L. L., Schauffler, S. M., Stell, M., Tilmes, S., Ullmann, K., Weinheimer, A. J., Akiyoshi, H., Chipperfield, M. P., Deushi, M., Dhomse, S. S., Feng, W., Graf, P., Hossaini, R., Jöckel, P., Mancini, E., Michou, M., Morgenstern, O., Oman, L. D., Pitari, G., Plummer, D. A., Revell, L. E., Rozanov, E., Saint-Martin, D., Schofield, R., Stenke, A., Stone, K. A., Visioni, D., Yamashita, Y., and Zeng, G.: Stratospheric Injection of Brominated Very Short-Lived Substances: Aircraft Observations in the Western Pacific and Representation in Global Models, *J. Geophys. Res.*, 123, 5690–5719, <https://doi.org/10.1029/2017JD027978>, 2018.
- 995 Williams, C. R.: Vertical air motion retrieved from dual-frequency profiler observations, *J. Atmos. Oceanic Technol.*, 29, 1471–1480, 2012.
- Wohltmann, I. and Rex, M.: The Lagrangian chemistry and transport model ATLAS: validation of advective transport and mixing, *Geosci. Model Dev.*, 2, 153–173, 2009.
- Zaucker, F., Daum, P. H., Wetterauer, U., Berkowitz, C., Kromer, B., and Broecker, W. S.: Atmospheric <sup>222</sup>Rn measurements during the 1993 NARE Intensive, *J. Geophys. Res.*, 101, 29 149–29 164, 1996.
- 1000